International Journal of Pharmaceutics 691 (2026) 126584

Contents lists available at ScienceDirect

International Journal of Pharmaceutics

journal homepage: www.elsevier.com/locate/ijpharm

Acidity changes in glycine and L-histidine buffers, mannitol, and their mixtures after freezing and lyophilization

Lukáš Veselý [a], Jan Ryšávka [a], Radim Štůsek [a], Behera Susrisweta [a], Jiří Zeman [b], Thomas Loerting [c], Dominik Heger [a,*]

[a] Department of Chemistry, Faculty of Science, Masaryk University, Kamenice 5, 625 00 Brno, Czech Republic
[b] Department of Pharmaceutical Technology, Faculty of Pharmacy, Masaryk University, Palackého tř. 1946/1, 612 00 Brno, Czech Republic
[c] Institute of Physical Chemistry, University of Innsbruck 6020 Innsbruck, Austria

A B S T R A C T

Freezing and lyophilization are commonly used methods for stabilizing pharmaceutical and biochemical formulations. However, these processes can introduce a variety of freezing-induced stresses that may lead not to stabilization, but rather to the destabilization of active molecules. One of the most significant of these stresses is freezing-induced acidity change, which has been shown to cause protein aggregation, loss of structural integrity, and increased chemical reactivity. While buffers are routinely used in liquid formulations to minimize pH fluctuations, several studies have demonstrated that certain buffers not only fail to maintain pH during freezing but may actively contribute to acidity shifts. In this study, we investigate the effects of cooling rate, initial pH, mannitol concentration, and lyophilization on acidity in glycine and L-histidine buffer systems in the solid state (both frozen and lyophilized) using UV–VIS spectroscopy and differential scanning calorimetry. Our results indicate that the freezing of amino acid buffers causes a slight increase in pH (basification); however, changes in acidity are not solely the consequence of freezing as they also occur during lyophilization. Notably, in L-histidine with mannitol at pH 7, lyophilization induces acidification of up to 4 units − opposite to the direction observed during freezing. Furthermore, we explore the correlation between vitrification of the freeze-concentrated solution and freezing-induced acidity changes, as quantified using the Hammett acidity function (H_2-). These findings may inform the rational design of more robust stabilization strategies.

1. Introduction

The stability of (bio)pharmaceuticals during manufacturing, storage, and distribution remains a major challenge in drug development, particularly for protein-based therapeutics. As the demand for biopharmaceuticals grows, so does the need for robust stabilization strategies such as freezing and lyophilization. Freezing and freeze-drying (lyophilization) of aqueous solutions is widely used in the production and preservation of (bio)pharmaceuticals. These techniques enable long-term stability of chemically and biologically sensitive compounds by halting degradation pathways, thereby offering flexibility in storage, transport, and manufacturing logistics (Bhatnagar et al. 2007, Krausková et al. 2016).

Freezing and lyophilization are widely implemented in biopharmaceutical workflows, with estimates suggesting that more than half of all drug products administered to patients undergo at least one freezing step during production (Kasper and Friess 2011). Despite their ubiquity, freezing and lyophilization remain complex, multistage processes involving several poorly understood parameters that can negatively affect product quality and result in incomplete recovery of the active pharmaceutical ingredient (API) (Van den Berg 1959, Van den Berg 1966, Murase and Franks 1989, Cavatur and Suryanarayanan 1998, Gomez et al., 2001).

Formulation excipients are critical in mitigating these risks. Among amino acid-based buffers, glycine and L-histidine are among the most frequently used in parenteral formulations approved for use in the European Union. Similarly, mannitol and sucrose are common stabilizers and bulking agents (Gervasi et al. 2018). Glycine contributes as both a buffer ($pK_{a,1} = 2.34$; $pK_{a,2} = 9.60$ (O'Neil 2013)), and a crystallizing cosolute (Pyne and Suryanarayanan 2001), while L-histidine provides effective buffering near physiological pH ($pK_{a2} = 6$ (O'Neil 2013)) and can also contribute with antioxidant and metal-chelating properties (Sundberg and Martin 1974, Wade and Tucker 1998). Sugars such as sucrose act as cryo- and lyo-protectants by replacing water and limiting molecular mobility (Slade et al., 1991), whereas mannitol is frequently used to improve cake structure, though its polymorphic behavior can introduce additional formulation challenges (Su et al., 2017). Interactions among these excipients can significantly affect phase behavior and crystallinity, further complicating formulation design (Pyne et al., 2003; Cao et al., 2013).

* Corresponding author.
E-mail address: hegerd@chemi.muni.cz (D. Heger).

https://doi.org/10.1016/j.ijpharm.2026.126584
Received 13 June 2025; Received in revised form 7 January 2026; Accepted 7 January 2026
Available online 8 January 2026

Even though formulation excipients are carefully selected to enhance stability, freezing, as the first step of lyophilization (Carpenter et al. 1997, Wang 2000) remains particularly critical due to its role in initiating physical and chemical changes that affect API stability). During freezing, ice formation removes solvent water, resulting in a distinct increase in solute concentration and the formation of a freeze-concentrated solution (FCS) (Kolhe et al., 2010b, Krausko et al., 2014, Roessl et al., 2015, Vetráková et al., 2019, Minatovicz et al., 2020). This FCS constitutes a chemically distinct environment that was shown to differ significantly in polarity (Heger and Klan 2007), ionic strength, and pH compared to the original solution (Takenaka et al. 2006, Sundaramurthi et al. 2010, Vetráková et al. 2017, Imrichova et al. 2019, Thorat and Suryanarayanan 2019, Koranne et al. 2020, Heger et al. 2023, Susrisweta et al., 2023, Štůsek et al. 2024, Veselý et al., 2024a). These changes have been shown to promote aggregation (Heger et al. 2005, Veselý et al., 2024b, Garncarzová et al. 2025) that can lead to protein degradation (Cohen et al. 2010, Thorat et al. 2020) and conformational destabilization (Gabellieri and Strambini 2003). Furthermore, photostability in the frozen or lyophilized state differs significantly from that in solution (Literak et al. 2003, Miller et al. 2003, Janga et al. 2018).

Freezing-induced acidity changes are especially important for APIs, as most of them are pH sensitive. These changes are induced either by 1) Selective crystallization of buffer components (Murase and Franks 1989, Vetráková et al. 2017, Thorat and Suryanarayanan 2019, Veselý et al. 2025) or 2) freeze concentration of buffer salts (Susrisweta et al. 2023). Both can lead to substantial acidification or basification (Veselý et al. 2021), depending on the buffer system used. For example, sodium phosphate buffers have been shown to undergo a drop in acidity due to preferential crystallization of basic salts (Van den Berg and Rose 1959, Gomez et al. 2001, Vetráková et al. 2017), this acidity drop reached up to 7 units depending on the initial pH and cooling rate. On the other hand, citrate buffer, which had been thought to be a suitable excipient for freezing and lyophilization, was lately shown to undergo acidification upon freezing (Susrisweta et al. 2023). This freezing-induced acidity change was explained by the combination of both mentioned mechanisms. At low pH, the mechanisms of freeze concentration lead to acidification, whereas at higher initial pH acidification was caused by the precipitation of a basic buffer salt similar to the case of sodium phosphate buffer (Susrisweta et al. 2023). Although buffers are included in formulations to resist such changes, their performance under frozen conditions is often compromised, as demonstrated above. Despite the widespread use of buffers and cryoprotectants, current formulation strategies often rely on empirical approaches, with limited mechanistic understanding of how parameters such as cooling rate, buffer type, and excipient concentration affect acidity during freezing and freeze-drying. As a result, unanticipated acidity shifts in the frozen or lyophilized state continue to pose a risk to product quality and API stability.

Acidity in the frozen state can be determined via UV–VIS absorption spectroscopy in transmission mode, using indicator molecules as probes (Heger et al. 2023). Similarly, solid state acidity of lyophiles can be determined via diffuse reflectance spectroscopy of the lyophilized powder, providing the protonation state of probe molecules as a stand-in for hydronium ion activity (Govindarajan et al. 2014, Vetráková et al. 2017, Lay-Fortenbery et al. 2024). However, the method has the possible drawback of results depending on indicator choice (Pudipeddi et al. 2008). NMR can likewise be utilized to observe an ionizable probe such as an amine or carboxylic acid (Li et al. 2021, Lay-Fortenbery et al. 2024), while also allowing for the quantification of residual water (Du and Su 2024).

In this study, we investigate how cooling rate, initial pH, and mannitol concentration influence the acidity of glycine and L-histidine buffer systems in the frozen state. We also examine the effect of lyophilization on the final pH of these systems, providing deeper insight into acidity dynamics throughout the freeze-drying process. These findings may help guide the development of more robust formulations for cold-chain and lyophilized pharmaceutical products.

2. Materials and methods

2.1. Materials

The following compounds were used: glycine (CAS-No[56-40-6], Sigma-Aldrich, USA), L-histidine (CAS-No[71-00-1], Sigma-Aldrich, USA), D-mannitol (CAS-No[69-65-8], Sigma-Aldrich, USA), D-(+)-Glucose (CAS-No[50-99-7], Sigma-Aldrich, USA), sucrose (CAS-No [57-50-1], PENTA, Czech republic), cresol red (CAS-No[1733-12-6], Sigma-Aldrich, USA), bromocresol green (CAS-No[76-60-8], Sigma-Aldrich, USA), and bromocresol purple (CAS-No[115-40-2], Alfa Aesar, Germany). Standardized buffers were used for pH electrode calibration (Hamilton DuraCal buffer, pH 4.01, 7.00, 10.01).

2.2. Methods

2.2.1. Solution preparation

Stock solutions of amino acids were prepared by dissolving the corresponding amount of glycine or L-histidine in deionized water to produce a 1 M or 0.1 M solution, respectively. Samples only containing buffers were prepared by diluting their stock solutions, while samples containing sugars were prepared immediately before measurement by dissolving the corresponding amount of the powdered sugar (due to storage concerns and the high concentrations). A small amount of an aqueous concentrated indicator solution (cresol red, bromocresol green, or bromocresol purple, $c_{Ind} \approx 10^{-5}$M) was added to each sample. pH was adjusted by dropwise addition of 1 mM – 1 M of NaOH or HCl solutions and was monitored using a Hamilton pH MiniTrode glass electrode connected to a Mettler Toledo FiveEasy Plus pH-meter.

2.2.2. Freezing

The preparation of samples involved 5 distinct freezing methods (summarized in Table 1). Liquid samples were transferred to plastic cuvettes (Kartell Art. 01939 10 mm optical path macro cuvettes, 4.5 mL max. volume), and subsequently frozen using one of the 5 freezing methods (A-E). In methods A, B, and C, samples were frozen in an ethanol-dry ice (EDI) bath at –20 °C for 60 min **(A)**, –40 °C for 45 min **(B)** or –50 °C for 30 min **(C)**. In method **D**, samples were frozen to –196 °C via immersion in liquid nitrogen (LN) until bubbling around the cuvette subsided (indicating that the sample had reached the temperature of the coolant). In method **E**, samples were frozen in an EDI bath at –40 °C for 45 min, measured, then cooled to –196 °C in LN.

2.2.3. Lyophilization

The lyophilization of samples was performed using the pilot-scale freeze dryer Epsilon 2-12D (Martin Christ, Germany). Liquid samples were initially pipetted into 20R tubular glass vials (SGD Pharma, France) and placed in the freeze dryer. The entire process consisted of 4 h of freezing (at a cooling rate of 0.5 °C/min), 36 h of sublimation, and 4 h of secondary drying (the total of 44 h). The process was carried out automatically according to the settings specified in Table 2 and is visualized in Fig. S1. At the end of lyophilization, the system was aerated, and the vials were sealed with lyophilization stoppers (Datwyler Pharma, Switzerland) and crimped (West Pharma, USA).

Table 1
Summary of utilized freezing methods including the chosen label (A–E), freezing temperature in °C, freezing time in minutes and the chosen coolant.

Method label	Temperature, °C	Residing time in the cooling bath, min	Coolant
A	−20	60	EDI bath
B	−40	45	EDI bath
C	−50	30	EDI bath
D	−196	~2	LN
E	−40; then cooled to −196	45; then ~ 2	EDI bath + LN

Table 2
Parameters of the lyophilization process by individual steps including the process phase, time, and chamber temperature and pressure.

Step	Process phase	Time, hh:mm	Temperature, °C	Pressure, mbar
1	Precooling	0:00	20	–
2	Freezing	2:00	−40	–
3	Freezing	2:00	−40	–
4	Sublimation	0:01	−40	0.12
5	Sublimation	0:59	−40	0.12
6	Sublimation	30:00	20	0.12
7	Sublimation	5:00	20	0.12
8	Secondary drying	0:01	20	0.018
9	Secondary drying	1:59	30	0.018
10	Secondary drying	2:00	30	0.018

2.2.4. Differential scanning calorimetry

Calorimetric measurements were performed using a PerkinElmer DSC 8000 differential scanning calorimeter. For each measurement, a 10 mg or 50 mg droplet was pipetted into an aluminum crucible and sealed with a lid. The sealed crucible was inserted into the sample chamber and measured against an empty sealed crucible used as the reference. The sample insertion temperature was 25 °C; the sample was then cooled at a selected cooling rate (Q = 0.5, 2.5, 5, 10, or 30 °C·min^{-1}) to −180 °C and subsequently heated to 25 °C at a heating rate of h = 30 °C·min^{-1}.

A linear baseline was subtracted from each thermogram to improve visual clarity. The onset temperature of each first-order transition was determined as the intersection between the extrapolated baseline preceding the transition and the tangent to the leading edge of the peak.

2.2.5. UV–VIS spectroscopy

The UV–VIS spectra of both frozen and aqueous samples were taken using an Agilent Cary 5000 UV–VIS-NIR spectrophotometer equipped with an Agilent Internal DRA 2500 integrating sphere. The integrating sphere allowed for the collection of light scattered by ice crystals within frozen samples. The wavelength range used during the measurements was 650–350 nm. Prior to freezing, samples were measured at room temperature to determine exact initial acidity and measured again immediately after removal from the cooling bath. The temperature of the sample during measurement was not directly controlled, however the spectra remained unchanged during measurement and the influence of possible temperature changes during transfer and measurement can be deemed negligible as each measurement took <15 s (measurements were taken at a rate of ≈ 1800 nm/min for a 300–400 nm wide spectrum). Measurements were taken to guarantee the sample stability within the time of measurement, see the Sample stability during the measurement cycles in the SI for details (Fig. S2 and Table S1).

Diffuse reflectance spectra of lyophilized samples were taken using an Agilent Cary 5000 UV–Vis-NIR spectrophotometer fitted with an Agilent Praying Mantis Diffuse Reflectance Accessory. The powder resulting from lyophilization was first homogenized in a sufficiently dry mortar and pestle and loaded into the Micro sample cup.

2.2.6. Data processing of UV–VIS spectra

Each spectrum of a sample in a liquid or frozen state was baseline-corrected using the spectrum of pure water (liquid samples) or pure ice (frozen samples). The spectra of lyophilized samples were corrected according to the reflectance spectrum of pure mannitol powder. To find the relative abundances of the indicator forms, a least-squares minimization procedure was applied to the baseline-corrected spectrum, utilizing the known spectra of the pure forms of the present indicator. For this purpose, the reference liquid pure form spectra were expressed in their molar absorption coefficients and thus used for the minimization procedure. For the frozen samples, the pure forms were measured as well and were scaled according to the ratio of molar absorption coefficients of the liquid spectra under the assumption that the ratios remain constant during freezing. From the linear fit coefficients, relative abundances were obtained, which were further used in Eq. (1) to calculate the Hammett acidity function (H_{n-}). Each spectrum was independently determined at least three times and averaged. Information for each specific sample is given in the Supporting Information. The standard error of the mean (SEM) was calculated and used as 1σ error.

2.2.6.1. The Hammett acidity function. The Hammett acidity function was used for the calculation of acidity from the absorption spectra acquired in both liquid ($H_{2-,RT}$) and frozen (H_{2-}) states. The Hammett acidity function allows for the determination of acidity through the ratio of differently protonated probe molecules with a known pK_a value. The H_{2-} is then equal to:

$$H_{2-} = pK_{a,\,Ind} + \log\left(\frac{c_{Ind^{2-}}}{c_{Ind^{1-}}}\right) \quad (1)$$

where pK_a represents the negative decadic logarithm of the dissociation constant of the applied indicator; the numerator and denominator of the logarithm are the relative abundances of the deprotonated and protonated forms of the applied indicator, respectively. The relative abundances are coefficients obtained from the fit normalized by their sum. The Hammett acidity function H_{n-} (denoted in the text as H_{2-}, since only diprotic indicators were employed) is used to describe the acidity of highly concentrated or solid samples. The value of the Hammett acidity function differs from electrochemically determined pH in concentrated solutions (where proton activity (a_{H^+}) is low) and approaches pH in dilute solutions. For acidity values present in this study, H_{2-} can be deemed essentially equivalent to pH.

The resulting value is then represented as change in acidity from the initial H_{2-} or pH at room temperature in Eq. (2), where:

$$\Delta H_{2-} = H_{2-} - H_{2-,RT} \quad (2)$$

with H_{2-} being the Hammett acidity values of the frozen sample and $H_{2-,RT}$ the value determined at room temperature. The value of $H_{2-,RT}$ was substituted for pH (determined using a glass electrode) in samples undergoing lyophilization.

2.2.6.2. The Kubelka-Munk function. Reflectance spectra were converted to absorbance using the Kubelka-Munk function through a MatLab (version R2023b) script. The spectrum of the sample was divided by the spectrum of the baseline (reflectance of pure mannitol powder), resulting in reflectance of the probe indicator. The Kubelka-Munk function ($F(R)$) at wavelength λ was then calculated in Eq. (3) as:

$$F(R) = \frac{1 - R^2}{2 \bullet R} \quad (3)$$

where R is the reflectance of the sample and $F(R)$ is the value of the Kubelka-Munk function, equivalent to normalized absorbance. The value of the Hammett acidity function was then calculated from the resulting absorbance spectra identically to those of frozen samples.

2.2.6.3. Analysis of variance. A two-way analysis of variance (ANOVA) was applied to select datasets. For results acquired from freezing amino acid buffers at varying mannitol concentrations, the data was first split by buffer and room temperature solution pH, providing 4 separate datasets. The two factors in the ANOVA were freezing temperature (freezing method A and C, two levels) and mannitol concentration (9–15 levels depending on data). The analysis was performed using the built-in statistical routine in Origin 2023 (Version 10.0).

3. Results

3.1. Freezing-induced acidity changes of amino acids solutions

3.1.1. Glycine

Freezing-induced acidity changes for 10, 25, and 50 mM glycine solutions (0.75, 1.88, and 3.75 mg/ml, respectively) were assessed over a pH range of 2–9 using freezing methods B, D, and E (see Table 1). Acidity changes with respect to pH are shown in Fig. 1 and the acidity values are listed in Table S2.

In 10 mM glycine solutions at pH 2, all samples acidified beyond the range of the utilized pH indicator ($H_{2-} < 0$), whereas samples frozen from pH 2.5 all acidified by $\Delta H_{2-} \approx -1.20$. Samples frozen from pH 3.6 using method B (green in Fig. 1) acidified by ≈ 0.25 units and those frozen using methods D and E (orange and black in Fig. 1) by ≈ 0.5 units. Samples frozen from basic pH values of 8 and 9 acidified: method E (−196 °C) resulted in only slight acidification (0 to –0.25 units), whereas methods B and D yielded more pronounced acidification of ≈ –1.5 units.

In 25 mM glycine solutions at pH 2, all samples acidified beyond the range of the utilized pH indicator ($H_{2-} < 0$). Samples frozen from pH 3.4 basified by ≈ 0.4 units for method B, ≈ 0.7 units for method D, and ≈ 0.8 units for method E. Samples frozen from basic pH values of 8 and 9 acidified, with method E (−196 °C) giving negligible basification of + 0.03 units for pH 8 and an acidification by ≈ −0.3 for pH 9. Methods B and D acidified more intensely by around −1 and −0.8 units, respectively.

In 50 mM glycine solutions at pH values of 2–4, prepared by method B (green in Fig. 1), freezing consistently led to acidification, while the samples prepared by method D (black in Fig. 1) led to comparably less acidification at acidic pH values < 3.5, and basification above this value. Method E (orange in Fig. 1) produced similar changes to method D, on average higher by approx. 0.3 units.

At near-neutral to basic pH (8–9), methods D and E (–196 °C and stepwise cooling) resulted in basification, which increased with initial pH. At pH 9 these samples basified by $\Delta H_{2-} > 0.75$, where acidity could not be accurately determined, as only a single form of the pH indicator was observed. Samples frozen using method B (–40 °C) basified the least, followed by a sudden acidification at pH 9.

3.1.2. L-Histidine

Freezing-induced acidity changes in 10 mM (1.55 mg/ml) and 50 mM (7.76 mg/mL) L-histidine solutions were determined across a pH range of 2–10 after freezing using methods B, D, and E (see Table 1). The changes in acidity relative to room temperature pH are shown in Fig. 2, with corresponding values provided in Table S3.

In general, L-Histidine samples exhibited freezing-induced basification, regardless of the cooling method employed. The exception to this observation were samples with initial pH values of 8.5 for 10 mM solutions prepared using all methods and pH 9 or 9.5 for 50 mM solutions prepared by cooling method D (−196 °C). In these cases, slight acidification was observed, with a decrease in pH of less than 0.5 units. The strongest basification, up to 1.50 units, was observed at initial pH values between 2 and 5. For 10 mM solutions the acidity change was not influence by the freezing method; the sole exception lies at observation at pH 6.5, where samples frozen using method B basified by ~0.75, while those using method D and E basified less by ~0.25 units. For 50 mM solutions, the acidity change varies more substantially depending on the cooling method. Cooling method B (−40 °C) showed the least basification, while cooling methods D (−196 °C) and E (stepwise cooling –40 °C → –196 °C) resulted in more pronounced basification of similar extent.

For 50 mM solutions, the extent of basification decreased between pH 5.0 and 6.5, reaching a minimum ΔH_{2-} of approximately 0.06 at pH 6.5 across all methods. From pH 7 to 8.5, moderate basification (0.25–0.50 units) was observed. At pH > 9, ΔH_{2-} could not be accurately determined for methods B and E as only basic form of the indicator was present in the spectrum. In contrast, acidification was observed for method D for samples with initial pH > 9.

3.2. Freezing aqueous sugars

Freezing-induced acidity changes in solutions of mannitol, sucrose, and glucose were determined for a pH range of 6–8 after freezing using methods A and C (see Table 1). The ΔH_{2-} values are depicted in Fig. S2, S3, and S4 and provided in Tables S4, S5, and S6. Overall, the observed trend for all sugars across all concentrations is a freezing-induced acidification with an increase in initial pH. While mannitol and sucrose reached at most $\Delta H_{2-} \approx -1$, the glucose samples even exceed this value. The H_{2-} data was scattered and only a weak concentration and temperature dependence was observed. On the other hand, a significant dependence on initial pH was recognized. These results are further detailed in the appropriate Supplemental Materials section.

3.3. Freezing amino acids with mannitol

3.3.1. Glycine and mannitol

Freezing-induced acidity changes resulting from methods A and C (see Table 1) starting from an RT pH values of 7 and 8, are shown in Fig. 3 for aqueous mixtures of 10 mg/mL (133 mM) glycine and 5–150 mg/mL (27–819 mM) mannitol. The exact acidity values are listed in Tables S7 and S8.

For samples frozen from pH 7 (Fig. 3A), pronounced variability in

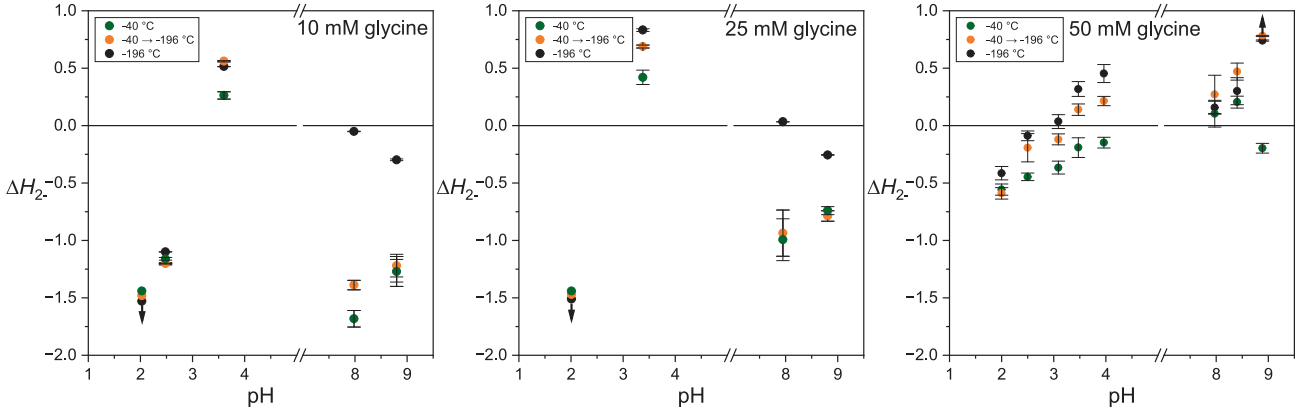

Fig. 1. Freezing induced acidity changes of 10 mM (left), 25 mM (center), and 50 mM (right) glycine prepared by cooling method B (green), D (black), and E (orange). Values represent mean ± standard error of the mean (SEM). Samples for which acidity could not be determined accurately — due to the presence of only one form of the pH indicator — are marked with an arrow indicating the interval boundary of possible acidity values.

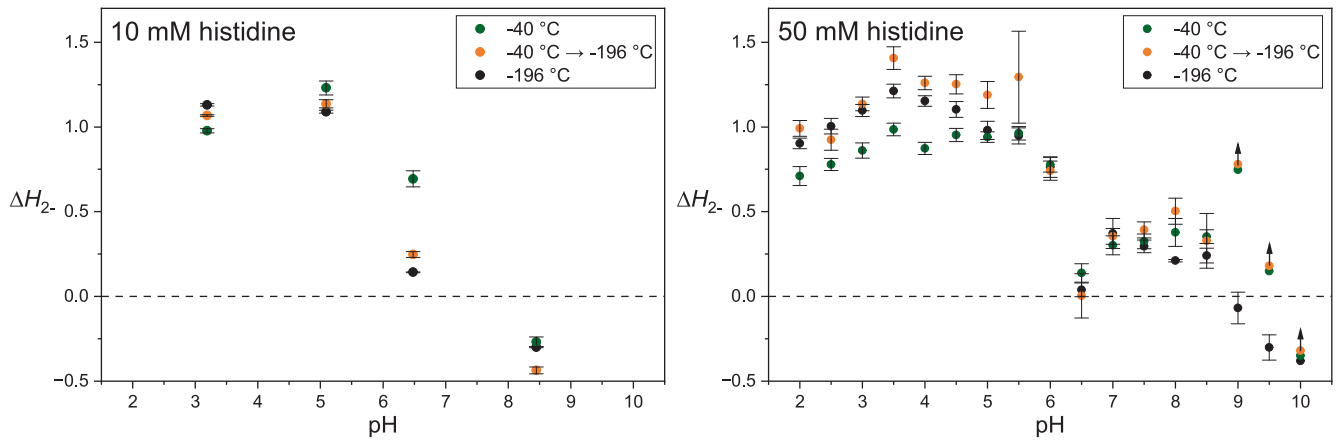

Fig. 2. Freezing induced acidity changes of 10 mM (left) and 50 mM (right) L-histidine prepared by cooling methods B (green), D (black), E (orange). Values represent mean ± SEM. Samples where acidity could not be accurately determined as only one form of the pH indicator was observed are indicated by an upwards arrow.

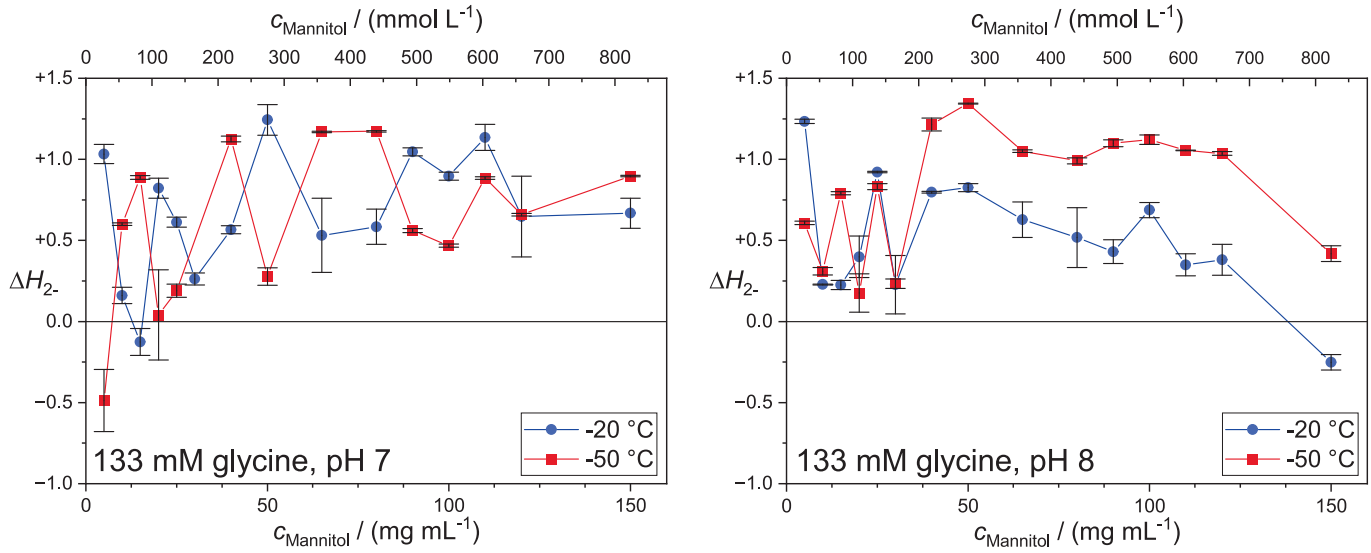

Fig. 3. Freezing-induced acidity changes in samples frozen from initial pH 7 (left) and pH 8 (right), using cooling methods A (blue) and C (red), containing glycine (10 mg/mL, 133 mM) and mannitol (5–150 mg/mL). Values represent mean ± SEM.

freezing-induced acidity changes was observed. Although no clear trend with freezing method can be seen between 5–80 mg/mL mannitol, basification generally increased with concentration, up to 50 mg/mL. For samples with a mannitol concentration higher than 80 mg/mL, the –20 °C freezing method (A) lead to less pronounced basification. The smallest difference between cooling methods occurs at 120 mg/mL mannitol, where both show similar basification of $\Delta H_{2-} \approx 0.65$. The greatest freezing-induced acidity change of +1.24 ± 0.09 units was observed at 50 mg/mL mannitol after freezing using method A. Two-way ANOVA indicated that, for samples containing glycine frozen from pH 7, mannitol concentration, but not cooling rate, significantly affected acidity changes, as addressed into more detail in section 4.4.

For samples frozen from pH 8 (Fig. 3B), ΔH_{2-} varied more strongly at lower mannitol concentrations (5–30 mg/mL), ranging from +1.23 ± 0.01 (5 mg/mL, method A) to 0.18 ± 0.12 (20 mg/mL, method C). Above 40 mg/mL mannitol, basification became more consistent. The largest shift was observed at 50 mg/mL mannitol (+0.83 ± 0.03 with method A and +1.34 ± 0.00 with method C). The overall minimum for acidity changes is present at the samples containing the largest mannitol concentration of 150 mg/mL, where the samples frozen using method C basified by 0.42 ± 0.05 units and the sample frozen using method A *acidified* by −0.25 ± 0.05 and is the only sample to have done so.

3.3.2. *L-histidine and mannitol*

Freezing-induced acidity changes resulting from freezing using methods A and C (see Table 1) from an RT pH of 7 and 8 for mixtures of 5 mg/mL L-histidine (32 mM) and 5–150 mg/mL mannitol (27–819 mM) are shown in Fig. 4 and the acidity values provided in Tables S9 and S10.

Samples with an initial pH of 7 (Fig. 4A) show consistent basification in a range of +0.69 and +1.04 units across all mannitol concentrations, regardless of freezing method.

In contrast, samples with an initial pH of 8 (Fig. 4B) initially showed similar basification regardless of freezing method. However, at 30 mg/mL, the acidity change diverged between freezing methods: samples frozen using method A basified by roughly half the extent compared to method B. Beyond 70 mg/mL mannitol, ΔH_{2-} values plateaued for both freezing methods.

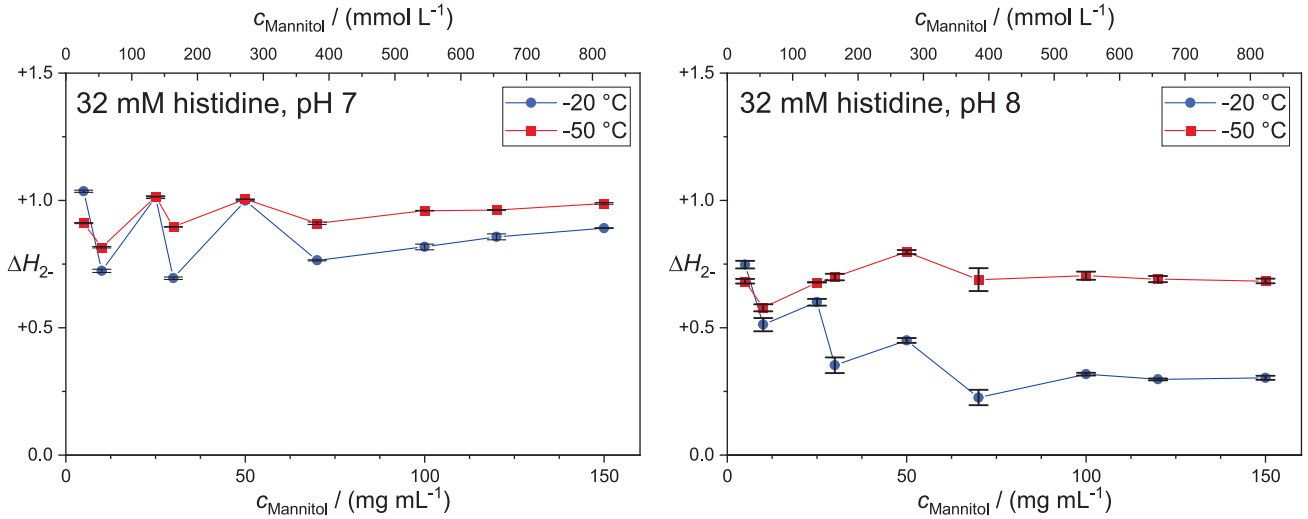

Fig. 4. Freezing-induced acidity changes in samples after freezing from initial pH 7 (left) and pH 8 (right), using method A (blue) and method B (red) ethanol-dry ice bath, containing L-histidine (5 mg/mL,. 32 mM) and mannitol (5–150 mg/mL). Values represent mean ± SEM.

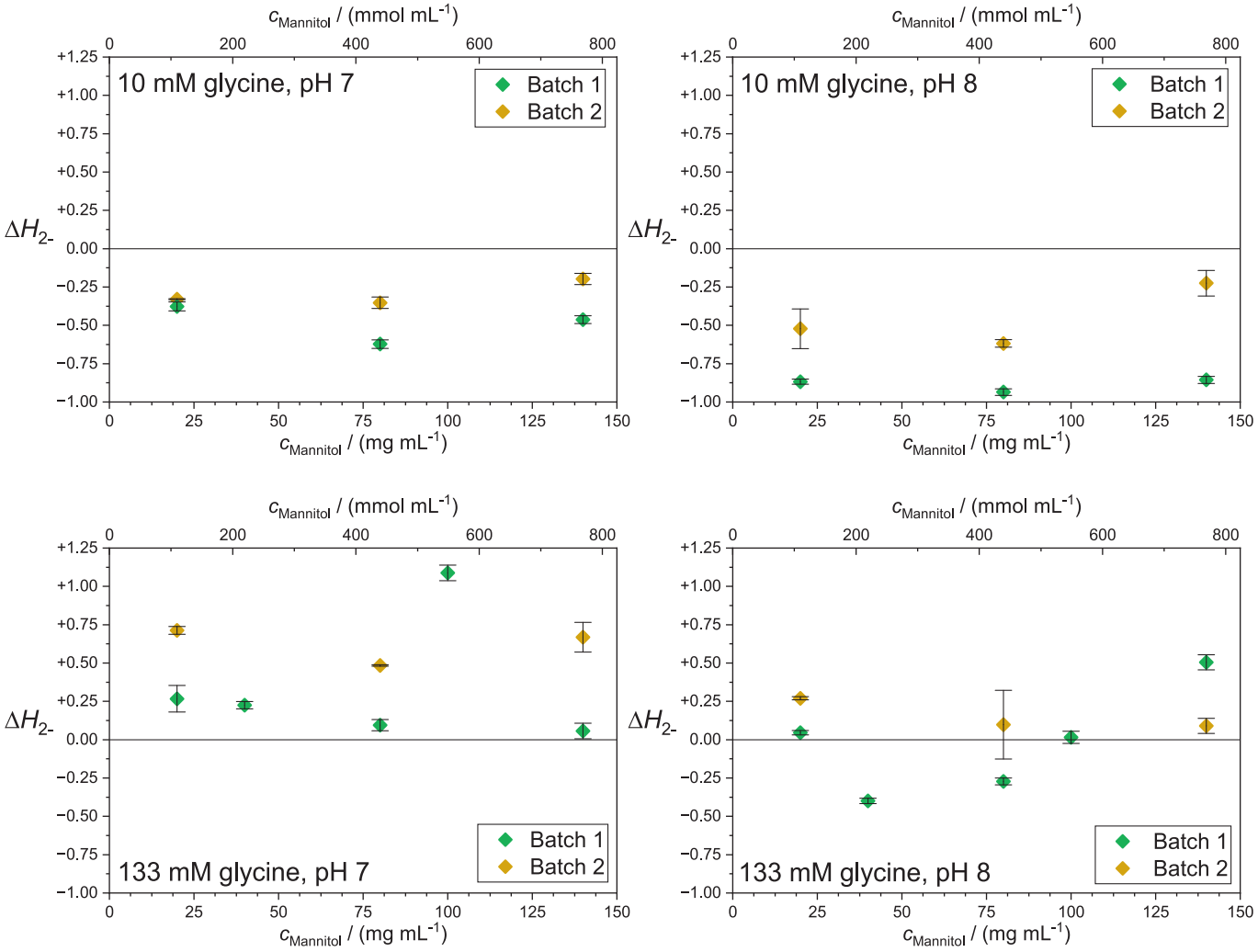

Fig. 5. Acidity changes in samples containing 0.75 mg/mL (10 mM, top) or 10 mg/mL glycine (133 mM, bottom) and mannitol (20–140 mg/mL) lyophilized from initial pH 7 (left) and pH 8 (right). Values represent mean ± SEM.

3.4. Lyophilization of amino acids with mannitol

3.4.1. Glycine and mannitol

Acidity changes after lyophilization from an RT pH of 7 and 8 for samples containing 0.75 and 10 mg/mL glycine (10 and 133 mM) and 20–140 mg/mL mannitol (110–769 mM), assessed for two independent batches, are depicted in Fig. 5 and the acidity values are provided in Tables S11–S14.

Solutions containing 10 mM glycine lyophilized from pH 7 (Fig. 5, top left) all mildly acidified by ≈ −0.25 to −0.50 units with a maximum difference between batches of ≈ 0.25 and the second batch acidifying slightly less. Solutions lyophilized from pH 8 (Fig. 5, top right) also acidified, although with a higher maximum of ≈ −1.0. The second batch also acidified less with a maximum batch-to-batch difference of 0.6 units.

All 133 mM glycine samples with initial pH 7 (Fig. 5, bottom left) basified following lyophilization. $\Delta H_{2\text{-}}$ values gradually decreased with increasing mannitol concentration (from to +0.25 at 20 mg/ml mannitol to +0.05 at 140 mg/ml mannitol), except for the sample with a mannitol concentration of 100 mg/mL, where a sudden spike in basification ($\Delta H_{2\text{-}} \approx +1$) was observed. In comparison, the second batch basified by approx. 0.5 units more than the first for repeated mannitol concentrations.

In 133 mM glycine samples with initial pH 8 (Fig. 5, bottom right), samples from the first batch underwent differing acidity changes depending on mannitol concentration: samples mildly acidified at 40 and 80 mg/ml mannitol (up to −0.4 units), at 20 and 100 mg/ml mannitol samples exhibited almost no acidity change, and at 140 mg/ml mannitol they basified by ≈ +0.5 units. However, samples from Batch 2 all basified by +0.1 to +0.25 units.

3.4.2. L-Histidine and mannitol

Acidity changes after lyophilization from an RT pH of 7 and 8 in solutions of 5 mg/mL L-histidine (32 mM) and 20–140 mg/mL mannitol (110–769 mM) are depicted in Fig. 6 and the acidity values are provided in Tables S15 and S16.

All samples with an initial pH of 7 (Fig. 6, left) acidified after lyophilization. Batch 1 exhibited large $\Delta H_{2\text{-}}$ values of −2.5 to −3. The most pronounced acidification ($\Delta H_{2\text{-}} = -2.93$) was observed for 140 mg/mL mannitol samples. Batch 2 acidified considerably less with values lying between −0.25 to −0.50 units.

In contrast, samples with initial pH 8 (Fig. 6, right) showed lower post-lyophilization acidification: Batch 1 acidified by up to −1 units with scattered results, while Batch 2 acidified similarly for all mannitol concentrations by −0.75 units.

3.5. Differential scanning calorimetry

3.5.1. Glycine

The aqueous solutions of glycine (c = 20 mg/mL = 266 mM) were prepared by cooling the solution with a rate of Q = 5, 10, 30 °C•min^{-1} (blue, green, and magenta, respectively in Fig. 7) and a constant heating rate h = 30 °C. Furthermore, a sample cooled by Q = 0.5 °C•min^{-1} and heated by h = 5 °C•min^{-1} (black in Fig. 7) was prepared to resolve some merged features contained in calorigrams using faster scans. The thermograms show several thermal features, a weak endothermic transition at −14 °C (−15.5 °C in case of the sample heated with 5 °C•min^{-1}), an endothermic transition at ≈ −3.8 °C and, finally, the main endothermic feature with an onset at ≈ 0 °C. The latter most likely corresponds to ice melting based on its large intensity and temperature close to that of ice melting. The endothermic transition prior to it should correspond to the glycine-H_2O eutectic melting temperature. The eutectic temperature resembles that of the β-glycine ($T_{e,\ \beta}$ = −3.6 °C (Drebushchak et al. 2013)), in particular the *β-glycine* polymorph is typically formed during freezing (Sundaramurthi and Suryanarayanan 2011). Finally, the weak endothermic feature at −15 °C has not been reported for glycine aqueous solutions, however, it is quite close to the eutectic temperature of sodium glycinate (−17 °C) (Akers et al. 1995). Since our samples had a pH of 6.30, the equilibrium ratio of glycinate to glycine should be approximately 1:1000. Therefore, we interpret this weak endotherm as the eutectic melting of the sodium glycinate. Interestingly, its intensity depends on the cooling rate, increasing as the cooling rate decreases. This can be interpreted as an increasing extent of glycinate crystallization at lower cooling rates (clearly visible in the inset of Fig. 7).

In our calorimetric observations, we have not detected any glass transition (and subsequent cold crystallization) of the glycine aqueous solution. In the literature, the glass transition is reported to be located at approx. −80 °C and followed by a cold crystallization (onset at approx. −60 °C) for 15 $\%_{w/w}$ glycine aqueous solutions with a cooling rate of 500 °C/min (Pyne and Suryanarayanan 2001). That is to say, the glycine solutions in this work crystallize upon cooling, but do not vitrify.

3.5.2. L-Histidine

The aqueous solutions of L-histidine (c = 5 mg/mL = 32 mM) were cooled by a cooling rate of 10 °C•min^{-1} and 0.5 °C•min^{-1} and subsequently heated at the rate of 30 °C•min^{-1}. The heating calorigrams revealed a complex glass transition behavior in the sample frozen at higher rate (10 °C•min^{-1}) (inset of Fig. 8). At least three features

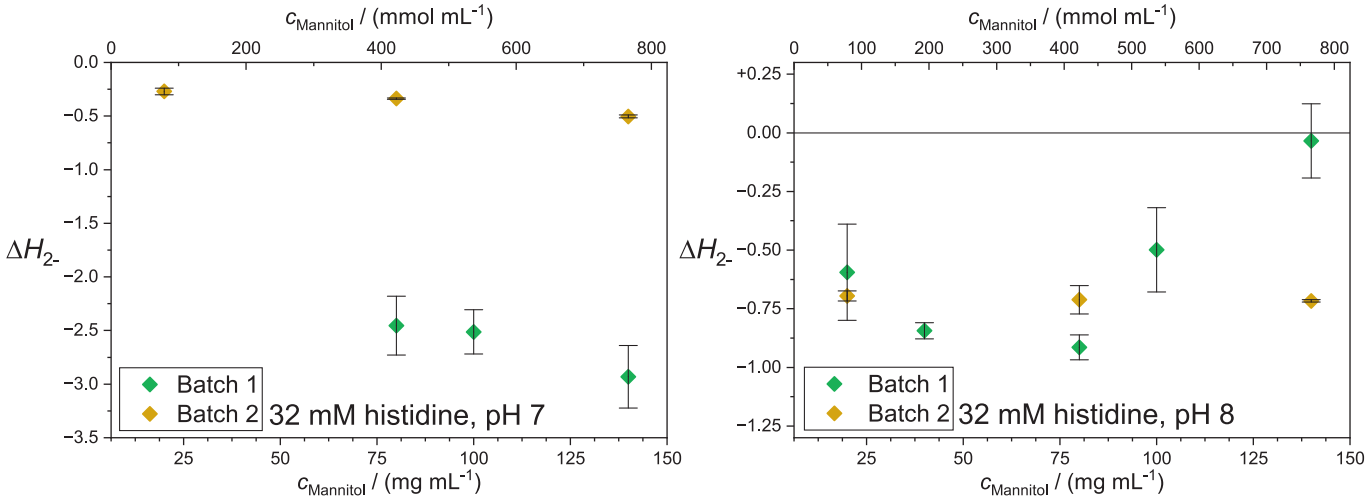

Fig. 6. Acidity changes in samples containing L-histidine (5 mg/mL, 32 mM) and mannitol (20–140 mg/mL) lyophilized from initial pH 7 (left) and pH 8 (right). Values represent mean ± SEM.

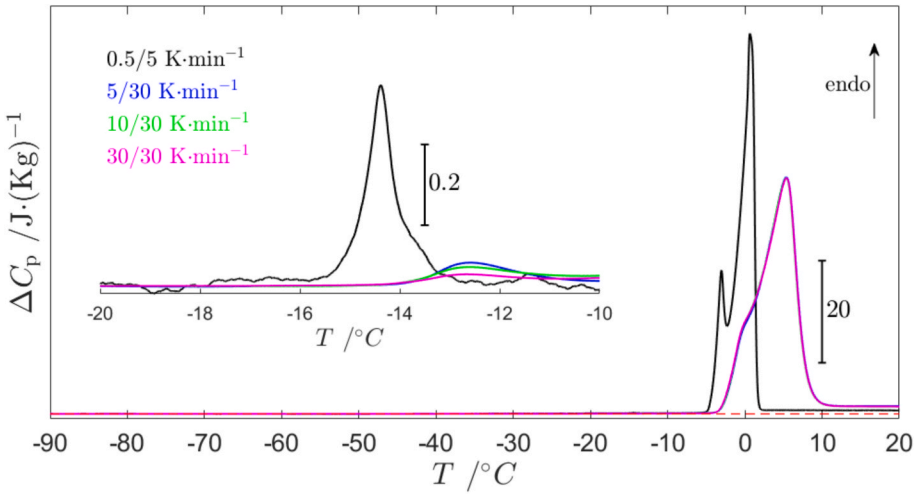

Fig. 7. The DSC heating scans of 20 mg/mL glycine solution cooled and heated with various rate combinations, which are shown in the legend in the format of *cooling/heating* rate. The thermal capacity (scaled according to the scalebar on the right of the largest peaks) is normalized to the mass of the sample ($m = 9.60$ mg in this case). The zero baseline is shown by the red dashed line for the main plot. The inset (corrected with different baseline for visual clarity) shows the endotherm located in the range of −20 and −10 °C and its ΔC_p scalebar is included on the right of the largest peak.

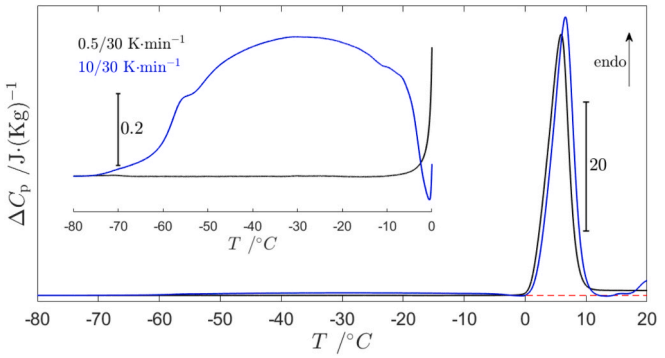

Fig. 8. The DSC heating ($h = 30$ K•min^{-1}) scans of 5 mg/mL L-histidine (pH = 7.8) solution cooled with 0.5 K•min^{-1} (black) and 10 K•min^{-1} (shown in the legend as *cooling/heating* rate). The inset plot shows the magnification of the scans in the range of −80 and 0 °C. The sample of lower cooling rate (0.5 K/min) shows no sign of vitrification, whereas the sample of faster cooling rate (10 K/min) shows a relatively complex vitrification behavior.

indicating a glass transition can be discerned. At approx. −75 °C, an onset of a first glass transition is seen, a second feeble glass transition shows an onset at approx. −65 °C, while the largest underlying glass transition seems to have an onset at approx. −70 °C. The probed samples had a pH of 7.8, in which a glass transition of approximately −30 °C have been reported (Österberg and Wadsten 1999). Unfortunately, no calorigrams are presented in the mentioned publication which disallows comparison with our calorigrams. Our data shows transitions at lower temperatures, which we tentatively interpret as three glass transitions of protonated (H_2His^+), neutral (HHis) and deprotonated (His^-) L-histidine.

The samples cooled more slowly ($Q = 0.5$ K/min) show no sign of vitrification making them fully crystalline. Compared to pure glycine solutions, L-histidine shows vitrification already at $Q = 10$ °C/min, whereas glycine solutions do not show any vitrification even at $Q = 30$ °C/min.

3.5.3. Glycine-mannitol mixtures

The aqueous solutions of glycine ($c = 10$ mg/mL) and mannitol ($c = 50$ mg/mL) mixture were cooled and heated by the same rate of $h = Q = 50$ °C/min to assess their thermal behavior. All the samples showed a glass transition close to approx. −60 °C, which is slightly higher than the observed glass transition of glycine solution (−80 °C). This difference is expected as the Gordon-Taylor equation predicts increase in T_g with increasing solute concentration (Gordon and Taylor 1952, Ondrušková et al., 2020). Following the first glass transition, we can observe a second, reproducible glass transition at approximately −40 °C, and a third glass transition observed in some samples, and it is in some cases followed by an exothermic feature, most likely a cold crystallization. Both second and third glass transitions originate from mannitol as they are present in both glycine-mannitol and L-histidine-mannitol mixtures. Overall, the mixture of glycine and mannitol showed variability (Fig. 9) between each DSC scans, as the third glass transition is not present in one of the samples (black), and when it occurs (green), either ice melting or a cold crystallization follow.

3.5.4. L-Histidine-mannitol mixtures

The aqueous solutions of L-histidine ($c = 5$ mg/mL = 32 mM) and mannitol ($c = 100$ and 50 mg/mL) mixtures were cooled by several cooling rates ($Q = 2.5$, 10, 50 °C•min^{-1}) and heated by either 30 or 50 °C•min^{-1} to assess their thermal behavior. The heating scans (Figs. 10 and 11) show that regardless of the cooling rate, two significant endothermic features (approx. −28 °C and –22 °C) can be observed for both the higher ($c = 100$ mg/mL) (Fig. 10) and lower (c = 50 mg/mL) (Fig. 11) mannitol concentrations. Following the second endotherm, there is an exothermic feature, most likely a cold crystallization. This exotherm is the most intense. For the sample cooled at 10 °C/min for both sugar concentrations. Additional feeble transitions having an onset of approx. −60 °C, which is most likely the glass transition of L-histidine (Hauptmann et al., 2021) and for the 10 K/min cooled sample there is a crystallization observable. The only remaining feature is ice melting merged with the eutectic melting near 0 °C.

The two endotherms located in the temperature range of −30 to −20 °C are common for the mixtures of both glycine-mannitol and L-histidine-mannitol. Therefore, these endotherms are most likely the glass transition temperatures of mannitol (Rodrigues, Rego et al. 2021), which evidently undergoes the first glass transition, forming a viscous liquid, then a second glass transition follows, after which a cold crystallization is initiated in some cases. For the cooling rate of 10 K/min, the largest cold crystallization is observable (along with the L-histidine cold crystallization), although for the sample cooled and heated with the rate of 50 K•min^{-1} a cold crystallization is still noticeable.

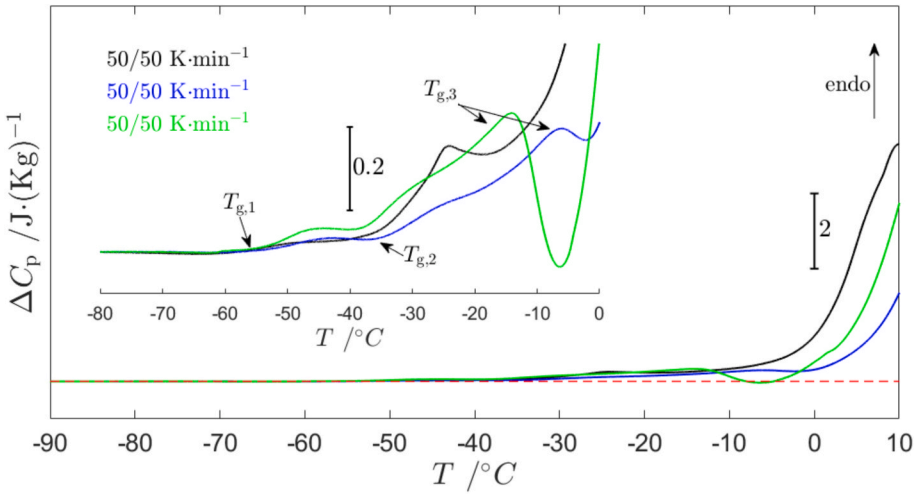

Fig. 9. The DSC heating scans (h = 50 °C•min-1) of glycine-mannitol mixture (c = 10 mg•mL-1 and 50 mg•mL-1, respectively) cooled by the rate of 50 °C•min-1. The inset shows the complex glass transition behavior in the range of −80 °C to 0 °C. In the inset, three glass transitions are denoted by increasing temperature.

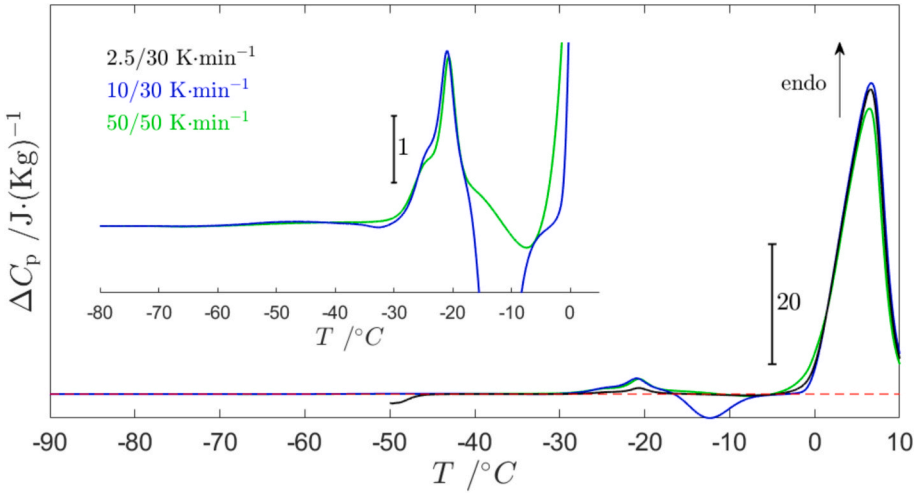

Fig. 10. The DSC heating scans of L-histidine-mannitol (c = 5 mg/mL and 100 mg/mL, respectively) cooled and heated with a rate combination shown in the upper right of the plot. The inset plot shows the complex glass transition behavior in the range of −80 °C to 0 °C.

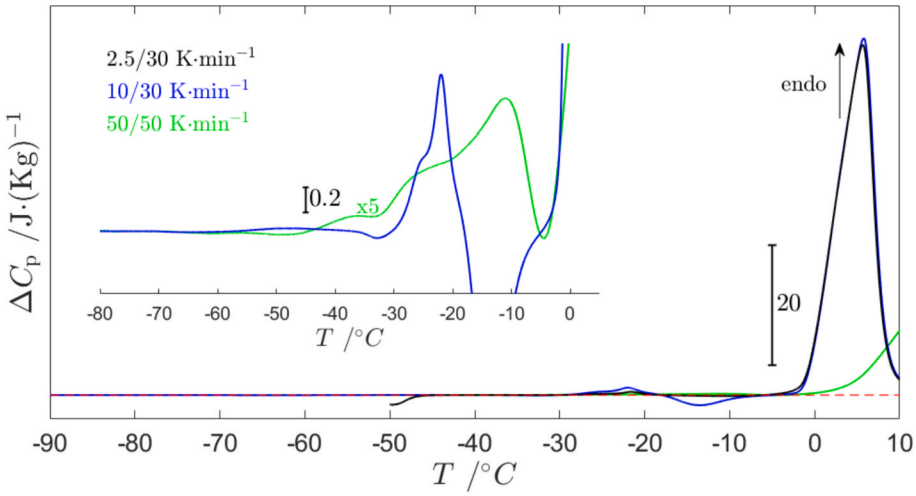

Fig. 11. The DSC heating scans of L-histidine-mannitol (c = 5 mg/mL and 50 mg/mL, respectively) cooled and heated with a rate combination shown in the upper right of the plot. The inset plot shows the complex glass transition behavior in the range of −80 °C to 0 °C.

4. Discussion

Freezing-induced acidity changes of buffers can often jeopardize the stability of biomolecules or APIs. However, insufficient attention has been paid to this phenomenon. This work first focuses on the assessment of freezing-induced acidity changes of glycine and L-histidine with respect to initial pH and cooling method. Second, we focus on freezing-induced acidity changes in glycine and L-histidine solutions combined with mannitol, considering the individual contributions of initial pH, cooling rate, and mannitol concentration. Third, the acidity of these mixtures is also assessed after lyophilization, where effects of initial pH and mannitol concentration are examined.

4.1. Solid state acidity measurements

Several methods have been used to determine acidity in the frozen and/or lyophilized state, including electrochemical measurements (Sundaramurthi and Suryanarayanan 2011, Thorat et al. 2020), optical spectroscopy (Kataoka et al. 2021, Veselý et al. 2021, Štůsek et al. 2024), and solid state nuclear magnetic resonance spectroscopy (SSNMR) (Li et al. 2021, Du et al. 2024, Lay-Fortenbery et al. 2024). The electrochemical method most commonly employs a low-temperature electrode, which has been shown to be reliable for liquid samples at low temperatures and applicable for partially crystalline and partially liquid samples (slurry method) (Pudipeddi et al. 2008). However, during freezing the pH electrode is affected by the insufficient amount of the liquid phase (Du et al. 2024), resulting in a deviation of several pH units compared to acidity assessed by other means, including an in-situ UV–Vis or SSNMR probe placed within the freeze-concentrated solution, which more reliably reflects the acidity (Hammett acidity function, H_{2-}) of the environment where the active molecules reside.

The probe method has also been shown to give reliable results for lyophilized samples. Furthermore, it has been proposed as a reliable empirical scale for predicting solid-state incompatibility with acid-sensitive APIs (Govindarajan et al. 2014). Recently, comparisons between the UV–Vis probe method and SSNMR showed that the resulting relative acidities did not differ significantly (Lay-Fortenbery et al. 2024).

In this work, we use the UV–Vis probe method to assess the Hammett acidity function (H_{2-}) of samples in frozen and lyophilized states. Our method probes the acidity of the FCS between ice crystals or the surface acidity of ice crystals and precipitated excipients in the frozen state, and the surface acidity of excipients in the lyophilized state. Therefore, the acidity we measure represents the average acidity of the portion of the sample through which the light penetrates.

Previous studies have shown that Hammett acidity changes with ionic strength. In highly ionic media, as is frequently the case for FCS, two major effects drive this change. First, the proton activity increases, which increases the apparent acidity of the sample. Second, the pK_a of the indicator shifts with ionic strength: it was shown to decrease from dilute to moderate ionic strength (roughly 1 M monovalent salt (NaCl, KCl, etc.)) and then increase again at higher ionic strengths. In frozen samples the temperature dependence of the indicator pK_a must be considered as well, as it was shown to increase with decreasing temperature. This likewise increases the apparent acidity, because lower acidity is required to produce the same amount of the basic form of the indicator. With a correctly chosen indicator and a properly determined pK_a for that indicator, the acidity can be assessed with an accuracy of $\pm$0.2 units. A more detailed discussion of the method and its limits can be found in detail in our previous publication (Veselý et al., 2024a).

4.2. Intra- and inter-vial variability of lyophiles

The difference in acidity within sections of the cake was assessed in one batch of lyophilized samples (in total of 22 vials). The lyophilized material within the vial was collected in vertical circular sections as depicted in Scheme 1 by different textures. The value of H_{2-}(Section) represents the acidity value of one particular section of the cake. The value H_{2-}(Vial) represents the average values of H_{2-}(Section) for an individual vial. The difference between the section's acidity and a vials average is plotted in Scheme 1 for a solution of 10 mg/ml glycine with 80 mg/ml mannitol with initial pH 7. The same data, plotted in a way to show absolute differences, are given in Fig. S6. Each section slightly deviates from the mean with no discernable trend. More detailed intra-vial variability data is presented in Table S17 and the depth-profiling data are shown in Table S18.

Overall, the intra-vial variability was negligeable with a maximum range of 0.21and a mean range for a total of 22 vials of 0.08 $\pm$ 0.01. This range is well within the experimental error (see above). Hence the overall results for lyophilized samples are presented as one average of all vials processed from one batch along with the standard error of the mean.

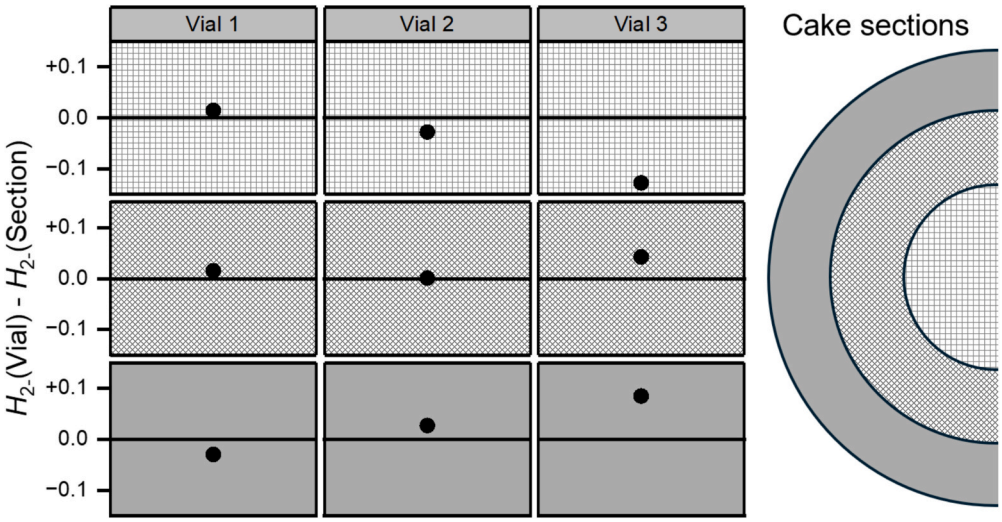

Scheme 1. H_{2-} variability depending on the region of the lyophilized cake for an example of 133 mM glycine with 80 mg/ml mannitol with an initial pH 7. On the right is a diagram of a top-view of a lyophilized cake, divided into shaded sections, which correspond to rows within the plot array on left. There, rows correspond to individual vials containing the same sample. The plot shows the difference in H_{2-} value for each section from the average of the whole vial, this average is equivalent to the zero-line.

4.3. Impact of initial pH and cooling rate

To understand freezing-induced acidity changes as a function of the initial room-temperature pH, it is essential to consider the speciation of the buffer components. In here we examined two common buffers: glycine with two pK_a values (p$K_{a,1}$ = 2.34; p$K_{a,2}$ = 9.60 (O'Neil 2013)) and L-histidine with three pK_a values (p$K_{a,1}$ = 1.82; p$K_{a,2}$ = 6.00; p$K_{a,3}$ = 9.17 (O'Neil 2013)).

Glycine exists in three distinct forms: an acidic form below p$K_{a,1}$ with the amine group protonated, a zwitterionic form between p$K_{a,1}$ and p$K_{a,2}$ with deprotonated carboxyl group while the amine remains protonated, and a negatively charged basic form above p$K_{a,2}$ with the carboxylic group deprotonated.

L-histidine has four distinct forms: below p$K_{a,1}$ the amine and imidazole groups are both protonated (the molecule has a net charge of +2), between p$K_{a,1}$ and p$K_{a,2}$, the carboxyl group is deprotonated and the amine and imidazole both protonated (+1 net charge), between p$K_{a,2}$ and p$K_{a,3}$ the carboxyl group is deprotonated, and the amine protonated (neutral zwitterion). Above p$K_{a,3}$, the carboxyl group is deprotonated (–1 net charge). The speciation of both amino acids is shown in Scheme 2, and the relative concentrations are depicted in Fig. 12.

4.3.1. L-histidine

L-histidine is widely employed as a multifunctional stabilizer in protein formulations (Al-Hussein and Gieseler 2013), due to its convenient buffering capacity in the physiological pH range and ability to maintain an amorphous state under certain conditions (Österberg and Wadsten 1999). However, freezing introduces physicochemical challenges that alter buffer behavior (Sundaramurthi et al. 2010, Vetráková et al. 2017, Thorat and Suryanarayanan 2019, Heger et al. 2023, Susrisweta et al. 2023, Veselý et al. 2025) and potentially impact protein stability (Pikal-Cleland and Carpenter 2001, Cao et al. 2003, Chen and Cui 2006, Krausková et al. 2016).

In the case of L-histidine, freezing-induced basification was observed, which is particularly pronounced in samples with initial pH values below 6 (as shown in Fig. 2). This basification is consistent with previous studies (Kolhe et al., 2010a, Sundaramurthi and Suryanarayanan 2011) and can be attributed to the precipitation of the acidic form of L-histidine (H_2His^+) during freezing (Sundaramurthi and Suryanarayanan 2011), which results in the removal of protons from the remaining liquid phase (FCS), thereby increasing basicity. The correspondence between the extent of basification and the speciation of L-histidine with respect to pH at room temperature can be illustrated with the help of Fig. 12 (right). Interestingly, in 50 mM samples, stepwise cooling (from –40 °C to –196 °C) resulted in the most pronounced basification at low initial pH values, likely due to enhanced cryoconcentration of the basic FCS following the crystallization in the first cooling step.

Samples of pH > p$K_{a,2}$, particularly above pH 6, exhibit only negligible acidity change after freezing. Vitrification of the FCS would lead to negligible acidity changes. Previous studies showed the enhanced ability of L-histidine to vitrify in vicinity of the second pK_a (Österberg and Wadsten 1999) and we have calorimetrically observed very intense glass transitions for samples cooled with a mild cooling rate of 10 °C·min^{-1} (blue in Fig. 8), although compared to the original article, our transitions occurred at much lower temperatures (−80 to -60 °C compared to −40 °C to 30 °C in the original (Österberg and Wadsten 1999)). On the other hand, the lower cooling rates of 0.5 °C·min^{-1} resulted in no vitrification (black in Fig. 8). Furthermore, cooling in the −40 °C bath likely exhibits cooling rate of 5–10 °C/min (Veselý et al., 2024b), while freezing in liquid nitrogen shows even higher cooling rates of approx. 1000–300 °C/min (Ondrušková et al., 2020), which would make the FCS amorphous. Given this, we can see in Fig. 2 that the acidity values are indistinguishable in the initial pH range of 6.5 to 8.5, therefore the dependence on the cooling method/cooling rate is no longer present, as was suggested in the literature for phosphate buffers (Murase and Franks 1989). The independence of resulting acidity value on cooling rate then immediately suggests that vitrification occurred, which is further supported by the likeness of the initial pH values and acidity after freezing.

The small difference can possibly be ascribed to the temperature dependent change of pK_a, it was previously shown that the pK_a can change by 0.3 by 15 °C (Daniele et al. 1985, Samuelsen et al. 2019). In the near neutral to basic pH range (pH 7–9), ΔH_2 remained small and positive regardless of freezing method. This suggests that L-histidine in this range exists predominantly in its neutral zwitterionic form.

4.3.2. Glycine

Glycine is widely used as both a buffering agent and a crystallizing agent in protein formulations (Pikal-Cleland et al., 2002; Ogienko et al. 2017) due to its ability to crystallize into stable polymorphs (Meyer et al. 2004, Xavier et al. 2020). During freezing, several glycine phases can be observed. The most common is the β-phase, which appears regardless of the initial pH of the solution (Varshney et al. 2007). At higher cooling rates, a glassy state of glycine can form; this metastable state then transforms into glycine dihydrate (previously known as the X-phase) upon warming (Xu et al. 2017). At extreme initial pH values or in the presence of salts, glycine can form either glycine hydrochloride or sodium glycinate. When more complex freezing methods are used (such as annealing at −20 °C or lyophilization) the γ-phase can also be detected. Furthermore, the crystallization of the neutral α-phase is inhibited by the presence of charged species, most importantly by the cation and anion of glycine itself, preferentially yielding the γ-phase (Towler et al. 2004).

Because of this complex phase behavior during freezing, glycine solutions can exhibit freezing-induced acidity changes that depend on both initial pH and cooling rate. In previous studies glycine was shown to basify upon freezing regardless of the initial pH. This change was assessed via low temperature pH electrode for relatively high buffer concentration (200 mM) and, were explained by preferential crystallization of acidic buffer components; glycine for high initial pH (pH > 9) or diglycine HCl in case of samples with low initial pH (pH = 3) (Sundaramurthi and Suryanarayanan 2011). In our study we have elaborated the impact of initial pH into more detail, and we have further added the concentration and cooling rate dependance on the freezing-induced acidity changes. Fig. 1 shows the dependence on all mentioned parameters. In the near vicinity and below the p$K_{a,1}$ (initial pH < 3), all samples acidified regardless of cooling method or the buffer concentration, with both cooling method and buffer concentration affecting the extent of acidification. Nonetheless, the acidification is

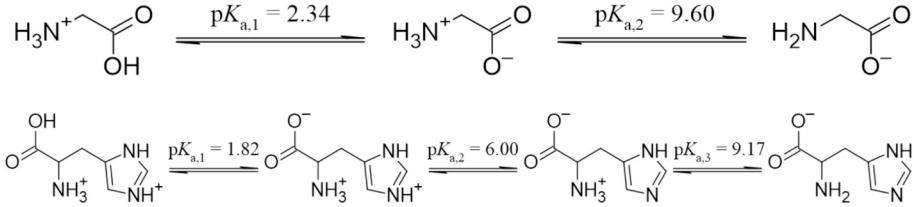

Scheme 2. The speciation of glycine (top) and L-histidine (bottom) with pK_a values included for each deprotonation reaction.

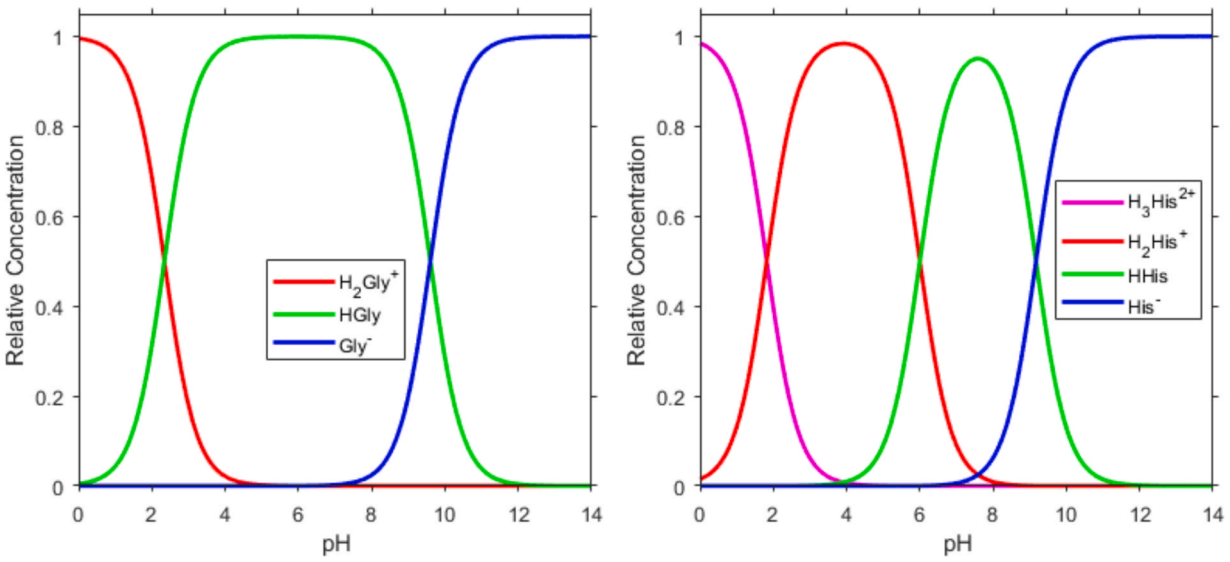

Fig. 12. Speciation diagrams of glycine (left) and L-histidine (right).

relatively mild due to large buffering capacity at this pH. The observed acidification could simply be explained as the freeze-concentration of the glycine HCl buffer component in the FCS. The extent of acidification gradually decreases with increasing concentration, thus eventually turning to basification as previously observed in (Sundaramurthi and Suryanarayanan 2011). Analogous behavior of freeze concentration of acid was observed for sodium citrate (Susrisweta et al. 2023) and PBS (Veselý et al. 2025).

Interestingly, sequential freezing (method E) provided intermediate acidity changes, likely reflecting partial crystallization during slow cooling, followed by vitrification of the rest of the FCS upon freezing in LN (method D). Furthermore, mannitol, or phosphate salts have been reported to inhibit glycine crystallization (Pyne et al. 2003), correlating with enhanced protein stability in lyophilized systems (Meyer et al. 2004, Liu et al. 2005). The phase behavior of glycine is also dependent on its speciation: glycine hydrochloride, glycine, and sodium glycinate exhibit different eutectic and glass transition characteristics (Meyer et al. 2004, Liu et al. 2005). Furthermore, cooling rate was shown to affect the phase behavior of glycine, where rapid cooling causes vitrification and slow cooling promotes the primary crystallization of glycine salts (Surovtsev et al. 2012). For the glycine solutions (c = 20 mg/mL) we have not observed any signs of vitrification, nonetheless slower cooling resulted in glycinate crystallization to a larger extent. In turn, a larger amount of crystallized glycinate relative to glycine would result in greater acidification. Indeed, on average the samples cooled in the ethanol bath (green in Fig. 1) are the most acidic. The difference would be even higher if the samples were frozen at −20 °C or higher.

At pH 8 and glycine concentration of 50 mM, the effect of cooling method diminished, which was not the case for more slowly cooled samples or samples of lower initial concentration (as shown in Fig. 1). The independence of cooling rate/method would again suggest vitrification. We are tentatively inclined to the possibility of glycine vitrification (at T_g = -70 to −85 °C) because of the minimal acidity change and no observable dependance on the freezing method, however our samples of 20 mg/mL glycine were slightly more acidic (pH 6.3) and more concentrated, thus we do not have a direct proof. We can show that glycine indeed tends to vitrify at cooling rates of 50 °C·min^{-1} with the addition of mannitol (see Fig. 9).

Vitrification kinetically traps the buffer components in an amorphous glassy matrix, thereby suppressing buffer precipitation and preserving the solution's acidity (see samples cooled in liquid nitrogen in Fig. 1, right), which changes at most by the temperature-dependent shift in pK_a. Previous studies showed that the neutral form of glycine tends to crystallize (which we observe in Fig. 7), whereas the salts (both glycine HCl, and sodium glycinate) tend to vitrify (Akers et al. 1995). The inclusion of sugars also promotes vitrification (see below). Fast crystallization of the neutral form explains the increased basification, however, the extent is only small due to the vicinity of the p$K_{a,2}$. The effect of partial vitrification on freezing induced acidity changes has been previously shown for HCl and PBS (Štůsek et al. 2024, Veselý et al. 2025). At higher pH values (pH 8.5 and 9), increased divergence between cooling conditions reappeared. Based on our results and previous studies of Akers, Milton et al. (1995), who observed the glass transition in the region of −70 to −85 °C, we hypothesize that some part of the sample is still liquid at –40 °C, and therefore, additional acidity changes occur after immersion of the sample into liquid nitrogen.

4.4. Aqueous glycine and L-histidine: Impact of mannitol concentration on freezing-induced acidity change

Sugars are often used as protein stabilizers in liquid, low temperature, and freeze-dried formulations. One of the most popular sugars applied in lyophilization is mannitol, which usually serves as a cryoprotectant and bulking agent (Izutsu et al., 1993), and is useful for example due to its high eutectic temperature of –2.24 °C (DeLuca and Lachman 1965). In general, it is thought that mannitol crystallizes well during freezing, however it was shown that the final state of frozen mannitol solutions is also dependent on other formulation components (Kim et al. 1998, Burger et al. 2000) and cooling rate (Rodrigues et al. 2021). However, studies investigating the effect of sugars on acidity changes in the frozen state remain scarce. To study the impact of mannitol on these changes, we chose samples with initial pH values of 7 and 8, based on their proximity to buffer pK_a values and the relevance of mild pH conditions typical for pharmaceutical formulations.

Freezing-induced acidity changes in samples at constant glycine concentration (10 mg/mL) and increasing mannitol concentrations (5–150 mg/mL) are shown in Fig. 3. The value of ΔH_2 initially fluctuates slightly above 0 for samples of both initial pHs. However, above 30 mg/mL of mannitol, consistent basification becomes more pronounced for both pH values. Considering the impact of freezing method, no apparent differences can be observed in pH 7 samples (Fig. 3, left), whereas for pH 8 samples (Fig. 3, right) method C (–50 °C EDI bath) led to increased basification compared to method A (−20 °C EDI bath).

Aqueous solutions containing only glycine at 3.75 mg/mL basify by 0–0.50 units from pH 8, as shown in Fig. 1. Thus, we observe that mannitol did not play a significant role up to a concentration of 30 mg/

mL; within experimental error, the extent of basification was similar in glycine solutions both with and without mannitol. However, basification became more pronounced and consistent at mannitol concentrations above 30 mg/mL. For pH 8 solutions the acidity increase is more pronounced above this concentration for method C (–50 °C) than method A (–20 °C), as shown in Fig. 3. Prior studies have shown that glycine crystallization kinetics are highly sensitive to formulation composition, with lower glycine concentrations, or the presence of amorphous stabilizers such as sucrose significantly delaying crystallization (Li and Nail 2005). Based on the DSC evidence (Fig. 9), cooling to −20 °C might lead to the crystallization of mannitol, whereas at −50 °C it would be amorphous, thereby affecting acidity.

The work by Pyne et al. (2003) reports that in the mannitol-glycine-water system with mannitol concentrations $c \geq 5\ \%_{w/w}$, the solutions tend to vitrify rather than crystallize. Indeed, our results are comparable to them, as Fig. 9 shows complex vitrification behavior for both glycine and mannitol. We therefore interpret the concentration dependence of mannitol on the acidity of frozen samples via vitrification. As discussed in the glycine and L-histidine sections, buffers were previously shown to vitrify more easily when the composition of the sample is close to the pK_a and other solutes are present. In our case, the observed basification by approximately 1 unit results in frozen state acidity close to glycine's pK_{a2}, further supporting the hypothesis that these samples underwent vitrification.

Additionally, acidity changes in the pH 8 glycine samples (Fig. 3, right) were dependent on cooling method: more pronounced acidity shifts occurred with method C (–50 °C) compared to method A.

For glycine frozen from pH 7 (Fig. 3, left), there was no significant difference in acidity change between the two freezing temperatures ($P = 0.92$, see the Analysis of variance chapter in the SI), whereas different mannitol concentrations produced significantly different acidity change values ($P < 0.0001$). In the averaged plot (Fig. 13), acidity changes increase sharply once mannitol concentration exceeds 30 mg/mL, which is slightly lower than the 5 $\%_{w/w}$ threshold for vitrification reported by Pyne, Chatterjee et al. (2003). A similar split also appears in the original data for glycine frozen from pH 8 (Fig. 3, right).

Freezing-induced acidity changes in L-histidine-mannitol solutions (Fig. 4) depended on initial pH and partly on mannitol concentration. In pH 7 samples (Fig. 4, left), all mannitol concentrations led to similar levels of basification ($\Delta H_{2\text{-}} \approx 0.7$–$1.0$), regardless of freezing method. pH 8 samples (Fig. 4, right) exhibited consistent basification when frozen using method C (–50 °C; $\Delta H_{2\text{-}} \approx 0.6$–$0.8$). Average acidity change

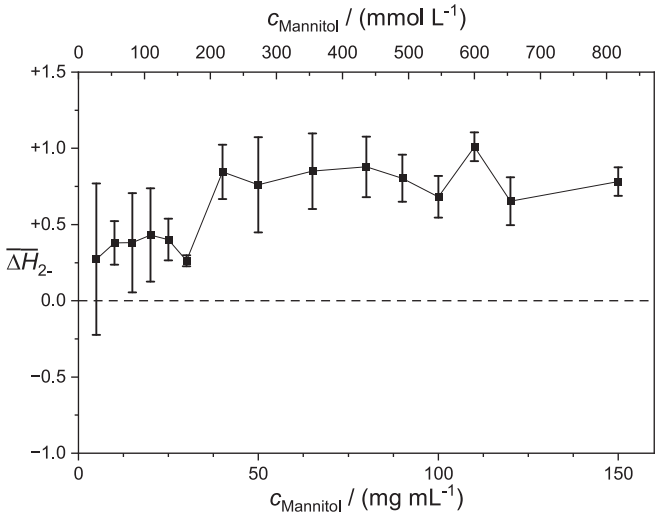

Fig. 13. $\Delta H_{2\text{-}}$ averaged for both freezing methods A and C (–20 and –50 °C EDI bath) of 10 mg/mL glycine frozen from initial pH 7 depending on present mannitol concentration (5–150 mg/mL).

across mannitol concentration for these samples is outlined in Table S23. Method A (–20 °C) led to results which were mannitol concentration dependent. Samples frozen using method A diverged in basification from method C above 25 mg/mL mannitol and basification dropped to $\Delta H_{2\text{-}} \approx 0.3$. In comparison, L-histidine solutions frozen using method B (–40 °C), basified by $\Delta H_{2\text{-}} \approx +0.3$–$0.4$ (Fig. 2). Such values were observed only for L-histidine-mannitol samples having RT pH 8, mannitol concentration above 25 mg/mL and prepared by method A. These results show that mannitol and L-histidine had a combined effect on basification. ANOVA was applied on the data sets discussed. For conditions under which L-histidine-mannitol solutions basified consistently upon freezing regardless of mannitol concentration, average $\Delta H_{2\text{-}}$ values are summarized in Table S18.

In our observations, glass transition events for mixtures of L-histidine and mannitol (Figs. 10 and 11) lie between the temperatures of the two freezing methods applied (−20 and −50 °C), indicating that vitrification can occur in the –50 °C-frozen samples. Furthermore, it was reported that the crystallization of L-histidine is suppressed when pH is closer to a pK_a value (Österberg and Wadsten 1999), since when pH nears a pK_a value, two species are distributed in a 1:1 ratio, leading to incompatibility for crystal lattice formation, reducing nucleation rate and favoring vitrification. Cryoconcentration during freezing drives the FCS acidity closer to L-histidine's $pK_{a,3}$ (9.17), where crystallization is suppressed, potentially further promoting vitrification.

This concentration-dependent behavior (Fig. 4, right) is comparable to that of the glycine-mannitol samples, where a critical concentration of mannitol of a similar value (~30 mg/mL) was observed, above which freezing-induced acidity changes differ from those of lower mannitol concentrations; furthermore, the temperature of freezing plays a role under these conditions. No detailed previous studies, such as DSC or X-ray of the L-histidine-mannitol-water system are available in the literature. However, we hypothesize that this sudden change in acidity points towards structural change within the frozen samples. Our examination of glycine and L-histidine conducted side-by-side in combination with mannitol suggests that vitrification is the primary reason, since the same shift in the glycine-mannitol-water system aligns with the onset of vitrification (Pyne et al. 2003).

4.5. *Lyophilization of glycine and L-histidine with mannitol*

When examining the impact of lyophilization on acidity changes, it should be considered that both cooling rate and freezing temperature have an impact on the state of frozen and lyophilized solutions (Kim et al. 1998, Mehta et al. 2013). Lyophilization was performed at a set cooling rate of 0.5 °C/min and the final lyophilization temperature was −40 °C. In comparison to utilized cooling methods (Table 1) a cooling rate of 0.5 °C/min is closest to method A (–20 °C EDI bath), while the final lyophilization temperature of –40 °C, is closer to method C (–50 °C EDI bath). Final temperature, cooling rate, and freezing temperature all influence the ratio of crystalline to amorphous solid in the final product.

4.5.1. *Concentration impact*

Lyophilization of glycine-mannitol mixtures led to acidification at lower glycine concentrations (10 mM, Fig. 5, top) and basification at higher concentrations (133 mM, Fig. 5, bottom). This behavior can be explained by acidity shifts in glycine-only solutions, where 10 and 25 mM glycine (left and middle panel of Fig. 1) acidifies from basic initial RT pH, whereas 50 mM glycine basified (right panel of Fig. 1). Meaning that lyophilization-induced acidity change mirrored the behavior of frozen solutions without mannitol.

4.5.2. *Batch variability*

Overall, variability in acidity changes between samples in an *individual* batch is low, as is apparent from the standard error of the mean (SEM) of individual graph points in Figs. 5 and 6, while batch-to-batch variability is more pronounced (see Batch 1 and Batch 2 in Figs. 5 and 6).

The highest difference between batches was observed for samples containing L-histidine and mannitol lyophilized from initial pH 7 (Fig. 6, left). Batch 1 acidified by up to ≈ −3.0 units, whereas Batch 2 acidified by a maximum of ≈ −0.5 units. If the T_g of the pH 7 histidine-mannitol was close enough to the lyophilization freezing step temperature (−40 °C), crystallization and vitrification would be both likely during freezing, which could possibly lead to vastly different acidity values. The vitrified samples would, presumably, keep acidity values close to those in the liquid state (Batch 1 in the left panel of Fig. 6), whereas crystallization of solutes would lead to a drastic change in acidity (Batch 2 in the left panel of Fig. 6). For pH 8, T_g was reported to be increased compared to pH 7 (Österberg and Wadsten 1999), leading to vitrification in both batches and thus similar acidification extent (Fig. 6, right). This batch-to-batch inhomogeneity also differs in comparison to frozen samples (Fig. 4), where freezing was performed in many individual runs for a range of mannitol concentrations while still providing consistent results when freezing to a lower temperature of −50 °C, further supporting the notion that inter-batch variability arises from the vicinity of the T_g to the lyophilization freezing temperature.

4.5.3. Comparison with frozen samples

Fig. 14 compares freezing-induced acidity changes with acidity changes of frozen and lyophilized samples containing 10 mg/mL glycine and 5–150 mg/mL mannitol. For samples lyophilized from pH 7 (Fig. 14, left), acidity shifts paralleled those in frozen samples, reaching a maximum of $\Delta H_{2\text{-}} = 1.08$ at 100 mg/mL mannitol, surpassing the corresponding value for freezing, before decreasing ($\Delta H_{2\text{-}} = 0.05$ in Batch 1, 0.66 in Batch 2) at 140 mg/mL. In lyophilized samples of initial pH 8 (Fig. 14, right), the mixture containing 20 mg/mL mannitol basified to a similar extent as the frozen sample, decreasing to a minimum of $\Delta H_{2\text{-}} = -0.40$ at 40 mg/mL, and then rose steadily to $\Delta H_{2\text{-}} = 0.50$ at the highest mannitol concentration (140 mg/mL, Batch 1). Overall, lyophilization from pH 8 resulted in lower acidity change compared to freezing and in some cases even in mild acidification.

These results are negative examples of the "pH memory" (Costantino et al. 1997, Vetráková et al. 2017), since specific samples frozen from both pH 7 and pH 8 exhibited almost no change in acidity in the lyophilized state, while presenting far greater acidity change in the frozen state (see Fig. 14, left, and Fig. 14, right, at 40 mg/mL mannitol).

Fig. 15 compares acidity changes in mixtures of aqueous L-histidine (5 mg/mL) and mannitol (5–150 mg/mL) frozen to –20 °C and –50 °C with lyophilized samples of the same composition. Lyophilization did not result in basification, as observed for frozen samples of the same composition, samples acidified instead. This cannot be attributed to differences in the freezing step, since for solution of L-histidine (7.76 mg/mL), the $\Delta H_{2\text{-}}$ varies by less than one unit between freezing temperatures of –40 °C and –196 °C (Fig. 2). Large acidity shifts were observed after lyophilization, reaching up to $\Delta H_{2\text{-}} \approx -2.93$ from pH 7 (Fig. 15, left) and $\Delta H_{2\text{-}} \approx -0.90$ from pH 8 (Fig. 15, right). Samples with RT pH 7 also present different acidity across batches (see above). This shows that the sublimation and secondary drying steps introduce additional chemical or structural changes. However our results are in agreement with previous ones, where acidification was observed for a mixture of trehalose and L-histidine after lyophilization (Lay-Fortenbery et al. 2024). The likely cause of acidification is the crystallization of the basic form of L-histidine ($HHis^+$) followed by devitrification at the heating step. Acidity shifts of this magnitude can be severely detrimental to APIs utilized in lyophilized formulations.

A difference in acidity between frozen and lyophilized samples was previously shown for Na-P and K-P buffers (Vetráková et al. 2017). However, the mechanism of lyophilization-induced acidity changes is not yet fully understood. In the frozen state, observed acidity corresponds to the acidity of the FCS, where APIs are located, however, after lyophilization we solely determine the surface acidity of excipients. Previously, surface acidity of lyophiles was linked to the degradation of several APIs (Govindarajan et al. 2006). Even though we do not offer a full explanation for observed acidity changes, we have discerned a distinct and large difference between acidity and overall trend in acidity changes between the liquid, frozen, and lyophilized state in L-histidine-buffered mannitol.

5. Conclusion

In this work, we assessed acidity changes induced by freezing and lyophilization in glycine, L-histidine, and their mixtures with mannitol, and related these shifts to phase transitions observed by DSC. Glycine solutions tended to crystallize even at high cooling rates (50 °C/min), whereas histidine solutions vitrified under relatively mild cooling (10 °C/min). In mixtures with mannitol, both systems exhibited pronounced solute vitrification at moderate to high sugar concentrations.

Final acidity was mainly governed by the sample's composition (components' concentration and initial pH) and cooling conditions, with acidity shifts arising from freeze-concentration, buffer precipitation, and (partial) vitrification. Vitrification appears to modulate acidity by

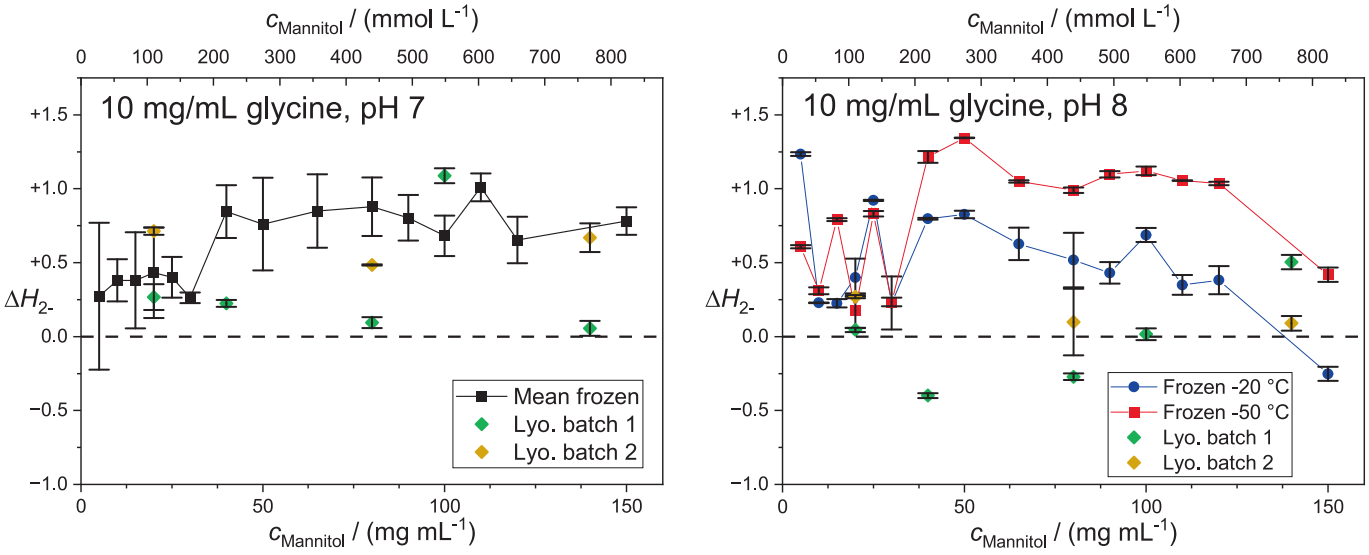

Fig. 14. Comparison of acidity changes in samples containing 10 mg/mL glycine and 5–150 mg/mL mannitol after freezing and lyophilization from initial pH 7 (left) and pH 8 (right). Values represent mean ± SEM.

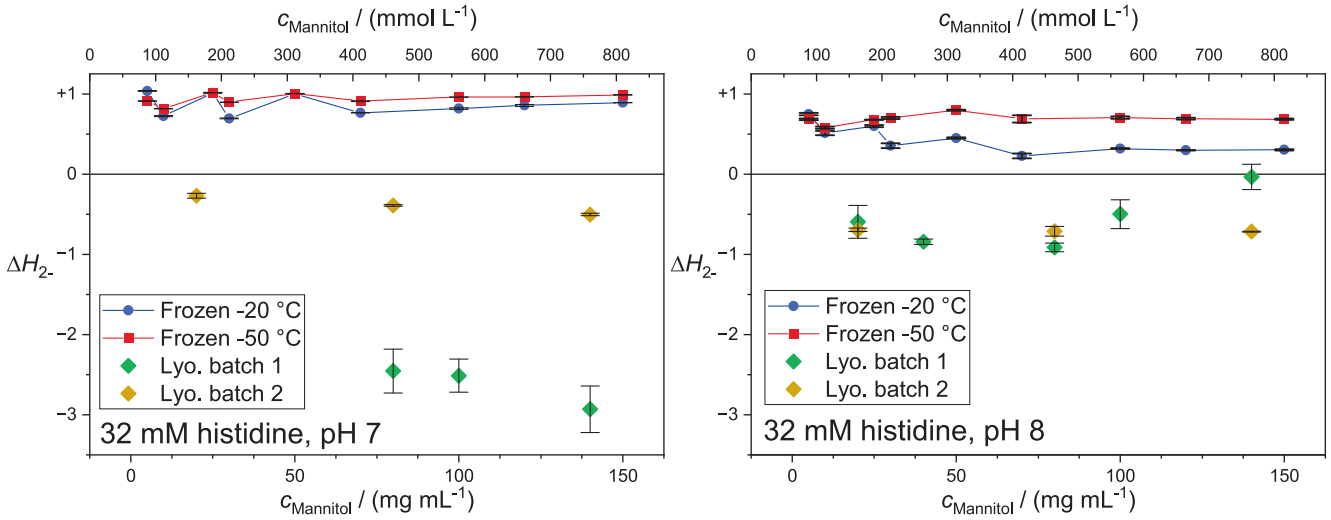

Fig. 15. Comparison of acidity changes in samples containing 5 mg/mL L-histidine and 5–150 mg/mL mannitol after freezing by cooling method A or C and after lyophilized from initial pH 7 (left) and pH 8 (right). Values represent mean ± SEM.

preventing the crystallization of solutes in the FCS and altering solute–solvent interactions. In buffer–mannitol mixtures, we identified a ~ 30 mg/mL mannitol threshold, above which freezing consistently caused basification, especially at –50 °C. Both glycine–mannitol and L-histidine–mannitol systems demonstrated a tendency toward vitrification; therefore, acidity changes in all cases remained within ~ 1 unit. Notably, acidity variability after freezing was lower in L-histidine–mannitol mixtures than in glycine–mannitol systems, indicating that glycine–mannitol formulations may be less suitable for frozen storage near neutral pH.

Lyophilization introduced additional, formulation-dependent acidity changes that diverged from frozen-state trends: glycine–mannitol mixtures showed a maximum basification at 100 mg/mL mannitol, while L-histidine–mannitol systems underwent strong acidification ($\Delta H_{2-} \approx -3$) at pH 7. Therefore, the combination of L-histidine and mannitol should be avoided in lyophilization formulations near neutral pH.

Overall, these presented results highlight that the concept of "pH memory" cannot be relied upon without considering the full multistage context of lyophilization, underscoring the critical roles of sublimation and secondary drying.

CRediT authorship contribution statement

Lukáš Veselý: Writing – original draft, Visualization, Methodology, Investigation, Data curation, Conceptualization. **Jan Ryšávka:** Writing – original draft, Visualization, Investigation, Data curation. **Radim Štůsek:** Writing – original draft, Methodology, Data curation. **Behera Susrisweta:** Writing – review & editing, Visualization, Investigation, Data curation. **Jiří Zeman:** Writing – review & editing, Methodology, Investigation, Data curation. **Thomas Loerting:** Writing – review & editing, Resources. **Dominik Heger:** Writing – original draft, Project administration, Methodology, Funding acquisition, Conceptualization.

Declaration of competing interest

The authors declare that they have no known competing financial interests or personal relationships that could have appeared to influence the work reported in this paper.

Acknowledgement

The research was supported by Czech Science Foundation via project GA25-15358S and to CEEPUS SI-1312-07-2425.

Appendix A. Supplementary material

Supplementary data to this article can be found online at https://doi.org/10.1016/j.ijpharm.2026.126584.

Data availability

Data will be made available on request.

References

Akers, M.J., Milton, N., Byrn, S.R., Nail, S.L., 1995. Glycine crystallization during freezing: the effects of salt form, pH, and ionic strength. Pharm. Res. 12 (10), 1457–1461.
Al-Hussein, A., Gieseler, H., 2013. Investigation of histidine stabilizing effects on LDH during freeze-drying. J. Pharm. Sci. 102 (3), 813–826.
Bhatnagar, B.S., Bogner, R.H., Pikal, M.J., 2007. Protein stability during freezing: separation of stresses and mechanisms of protein stabilization. Pharm. Dev. Technol. 12 (5), 505–523.
Burger, A., Henck, J.-O., Hetz, S., Rollinger, J.M., Weissnicht, A.A., Stöttner, H., 2000. Energy/temperature diagram and compression behavior of the polymorphs of d-mannitol. J. Pharm. Sci. 89 (4), 457–468.
Cao, E., Chen, Y., Cui, Z., Foster, P.R., 2003. Effect of freezing and thawing rates on denaturation of proteins in aqueous solutions. Biotechnol. Bioeng. 82 (6), 684–690.
Cao, W., Xie, Y., Krishnan, S., Lin, H., Ricci, M., 2013. Influence of process conditions on the crystallization and transition of metastable mannitol forms in protein formulations during lyophilization. Pharm. Res. 30, 131–139.
Carpenter, J.F., Pikal, M.J., Chang, B.S., Randolph, T.W., 1997. Rational design of stable lyophilized protein formulations: some practical advice. Pharm. Res. 14 (8), 969.
Cavatur, R.K., Suryanarayanan, R., 1998. Characterization of frozen aqueous solutions by low temperature X-ray powder diffractometry. Pharm. Res. 15 (2), 194–199.
Cohen, I.P.G., Castello, P.R., Flecha, F.L.G., 2010. Ice-induced partial unfolding and aggregation of an integral membrane protein. Biochimica et Biophysica Acta (BBA)-Biomembranes 1798 (11), 2040–2047.
Costantino, H.R., Griebenow, K., Langer, R., Klibanov, A.M., 1997. On the pH memory of lyophilized compounds containing protein functional groups. Biotechnol. Bioeng. 53 (3), 345–348.
Daniele, P.G., Rigano, C., Sammartano, S., 1985. Ionic strength dependence of formation constants—V: Protonation constants of some nitrogen-containing ligands at different temperatures and ionic strengths. Talanta 32 (1), 78–80.
DeLuca, P., Lachman, L., 1965. Lyophilization of pharmaceuticals I: effect of certain physical-chemical properties. J. Pharm. Sci. 54 (4), 617–624.
Drebushchak, V., Ogienko, A., Boldyreva, E.V., 2013. Polymorphic effects at the eutectic melting in the H2O–glycine system. J. Therm. Anal. Calorim. 111 (3), 2187–2194.
Du, Y., Li, J., Suryanarayanan, R., Su, Y., 2024. Probing chemical equilibrium in Frozen Sodium Phosphate Buffer solution by 31P solid-state NMR. J. Phys. Chem. Let. 15 (21), 5714–5720.
Du, Y., Su, Y., 2024. Quantification of residual water in pharmaceutical frozen solutions via 1H solid-state NMR. J. Pharm. Sci. 113 (8), 2405–2412.
Gabellieri, E., Strambini, G.B., 2003. Perturbation of protein tertiary structure in frozen solutions revealed by 1-anilino-8-naphthalene sulfonate fluorescence. Biophys. J . 85 (5), 3214–3220.

Garncarzová, M., Veselý, L., Kim, B., Kim, K., Heger, D., 2025. Spectroscopic characterization of phenol in frozen aqueous solution and on the ice surface. Spectrochim. Acta A Mol. Biomol. Spectrosc. 335, 125948.
Gervasi, V., Dall Agnol, R., Cullen, S., McCoy, T., Vucen, S., Crean, A., 2018. Parenteral protein formulations: an overview of approved products within the European Union. Eur. J. Pharm. Biopharm. 131, 8–24.
Gomez, G., Pikal, M.J., Rodriguez-Hornedo, N., 2001. Effect of initial buffer composition on pH changes during far-from-equilibrium freezing of sodium phosphate buffer solutions. Pharm. Res. 18 (1), 90–97.
Gordon, M., Taylor, J.S., 1952. Ideal copolymers and the second-order transitions of synthetic rubbers. I. Non-crystalline copolymers. J. Appl. Chem. 2 (9), 493–500.
Govindarajan, R., Chatterjee, K., Gatlin, L., Suryanarayanan, R., Shalaev, E.Y., 2006. Impact of freeze-drying on ionization of sulfonephthalein probe molecules in trehalose–citrate systems. J. Pharm. Sci. 95 (7), 1498–1510.
Govindarajan, R., Landis, M., Hancock, B., Gatlin, L.A., Suryanarayanan, R., Shalaev, E. Y., 2014. Surface acidity and solid-state compatibility of excipients with an acid-sensitive API: case study of atorvastatin calcium. AAPS PharmSciTech 16 (2), 354–363.
Hauptmann, A., Hoelzl, G., Loerting, T., 2021. Optical cryomicroscopy and differential scanning calorimetry of buffer solutions containing cryoprotectants. Eur. J. Pharm. Biopharm. 163, 127–140.
Heger, D., Govindarajan, R., Lu, E., Ewing, S., Lay-Fortenbery, A., Yuan, X., Veselý, L., Munson, E., Gatlin, L., Hancock, B., Suryanarayanan, R., Shalaev, E., 2023. Beyond pH: acid/base relationships in frozen and freeze-dried pharmaceuticals. Principles and Practices of Lyophilization in Product Development and Manufacturing. F. Jameel. Cham, Springer International Publishing: 39-61.
Heger, D., Jirkovsky, J., Klan, P., 2005. Aggregation of methylene blue in frozen aqueous solutions studied by absorption spectroscopy. J. Phys. Chem. A 109 (30), 6702–6709.
Heger, D., Klan, P., 2007. Interactions of organic molecules at grain boundaries in ice: a solvatochromic analysis. J. Photochem. Photobiol. A-Chem. 187 (2–3), 275–284.
Chen, Y.H., Cui, Z., 2006. Effect of salts on the freezing denaturation of lactate dehydrogenase. Food Bioprod. Process. 84 (C1), 44–50.
Imrichova, K., Vesely, L., Gasser, T.M., Loerting, T., Nedela, V., Heger, D., 2019. Vitrification and increase of basicity in between ice Ih crystals in rapidly frozen dilute NaCl aqueous solutions. J. Chem. Phys. 151 (1), 014503.
Izutsu, K., Yoshioka, S., Terao, T., 1993. Decreased protein-stabilizing effects of cryoprotectants due to crystallization. Pharm. Res. 10 (8), 1232–1237.
Janga, K.Y., King, T., Ji, N., Sarabu, S., Shadambikar, G., Sawant, S., Xu, P., Repka, M.A., Murthy, S.N., 2018. Photostability issues in pharmaceutical dosage forms and photostabilization. AAPS PharmSciTech 19, 48–59.
Kasper, J.C., Friess, W., 2011. The freezing step in lyophilization: Physico-chemical fundamentals, freezing methods and consequences on process performance and quality attributes of biopharmaceuticals. Eur. J. Pharm. Biopharm. 78 (2), 248–263.
Kataoka, S., Harada, M., Okada, T., 2021. Microscale pH inhomogeneity in frozen NaCl solutions. PCCP 23 (34), 18595–18601.
Kim, A.I., Akers, M.J., Nail, S.L., 1998. The physical state of mannitol after freeze-drying: effects of mannitol concentration, freezing rate, and a noncrystallizing cosolute. J. Pharm. Sci. 87 (8), 931–935.
Kolhe, P., Amend, E., Singh, S.K., 2010a. Impact of freezing on pH of buffered solutions and consequences for monoclonal antibody aggregation. Biotechnol. Prog. 26 (3), 727–733.
Kolhe, P., Holding, E., Lary, A., Chico, S., Singh, S.K., 2010b. Large-scale freezing of biologics: understanding protein and solute concentration changes in a cryovessel-Part I. Biopharm International 23 (6), 53–60.
Koranne, S., Lalge, R., Suryanarayanan, R., 2020. Modulation of microenvironmental acidity: a strategy to mitigate salt disproportionation in drug product environment. Mol. Pharm. 17 (4), 1324–1334.
Krausko, J., Runštuk, J., Neděla, V., Klán, P., Heger, D., 2014. Observation of a brine layer on an ice surface with an environmental scanning electron microscope at higher pressures and temperatures. Langmuir 30 (19), 5441–5447.
Krausková, L., Procházková, J., Klašková, M., Filipová, L., Chaloupková, R., Malý, S., Damborský, J., Heger, D., 2016. Suppression of protein inactivation during freezing by minimizing pH changes using ionic cryoprotectants. Int. J. Pharm. 509 (1–2), 41–49.
Lay-Fortenbery, A., Yuan, X., Veselý, L., Heger, D., Shalaev, E., Su, Y., Munson, E., 2024. Determination of solid-state acidity of lyophilized trehalose containing citrate, phosphate, and histidine buffers using UV/VIS diffuse reflectance and solid-state NMR spectroscopy. J. Pharm. Sci. 113 (12), 3479–3488.
Li, M., Koranne, S., Fang, R., Lu, X., Williams, D.M., Munson, E.J., Bhambhani, A., Su, Y., 2021. Probing microenvironmental acidity in lyophilized protein and vaccine formulations using solid-state NMR spectroscopy. J. Pharm. Sci. 110 (3), 1292–1301.
Li, X., Nail, S.L., 2005. Kinetics of glycine crystallization during freezing of sucrose/glycine excipient systems. J. Pharm. Sci. 94 (3), 625–631.
Literak, J., Klan, P., Heger, D., Loupy, A., 2003. Photochemistry of alkyl aryl ketones on alumina, silica-gel and water ice surfaces. J. Photochem. Photobiol. A-Chem. 154 (2–3), 155–159.
Liu, W., Wang, D.Q., Nail, S.L., 2005. Freeze-drying of proteins from a sucrose-glycine excipient system: effect of formulation composition on the initial recovery of protein activity. AAPS PharmSciTech 6 (2), 23.
Mehta, M., Bhardwaj, S.P., Suryanarayanan, R., 2013. Controlling the physical form of mannitol in freeze-dried systems. Eur. J. Pharm. Biopharm. 85 (2), 207–213.
Meyer, J.D., Jun Bai, S., Rani, M., Suryanarayanan, R., Nayar, R., Carpenter, J.F., Manning, M.C., 2004. Infrared spectroscopic studies of protein formulations containing glycine. J. Pharm. Sci. 93 (5), 1359–1366.
Miller, B.L., Hageman, M.J., Thamann, T.J., Barròn, L.B., Schöneich, C., 2003. Solid-state photodegradation of bovine somatotropin (bovine growth hormone): evidence for tryptophan-mediated photooxidation of disulfide bonds. J. Pharm. Sci. 92 (8), 1698–1709.
Minatovicz, B., Sun, L., Foran, C., Chaudhuri, B., Tang, C., Shameem, M., 2020. Freeze-concentration of solutes during bulk freezing and its impact on protein stability. J. Drug Delivery Sci. Technol. 58.
Murase, N., Franks, F., 1989. Salt precipitation during the freeze-concentration of phosphate buffer solutions. Biophys. Chem. 34 (3), 293–300.
O'Neil, M.J., 2013. The Merck Index: An Encyclopedia of Chemicals, Drugs, and Biologicals, Royal Society of Chemistry.
Ogienko, A.G., Bogdanova, E.G., Trofimov, N.A., Myz, S.A., Ogienko, A.A., Kolesov, B.A., Yunoshev, A.S., Zubikov, N.V., Manakov, A.Y., Boldyrev, V.V., Boldyreva, E.V., 2017. Large porous particles for respiratory drug delivery. Glycine-based formulations. Eur. J. Pharm. Sci. 110, 148–156.
Ondrušková, G., Veselý, L., Zezula, J., Bachler, J., Loerting, T., Heger, D., 2020. Using Excimeric fluorescence to study how the cooling rate determines the behavior of naphthalenes in freeze-concentrated solutions: vitrification and crystallization. J. Phys. Chem. B 124 (46), 10556–10566.
Österberg, T., Wadsten, T., 1999. Physical state of l-histidine after freeze-drying and long-term storage. Eur. J. Pharm. Sci. 8 (4), 301–308.
Pikal-Cleland, K.A., Carpenter, J.F., 2001. Lyophilization-induced protein denaturation in phosphate buffer systems: monomeric and tetrameric beta-galactosidase. J. Pharm. Sci. 90 (9), 1255–1268.
Pikal-Cleland, K.A., Cleland, J.L., Anchordoquy, T.J., Carpenter, J.F., 2002. Effect of glycine on pH changes and protein stability during freeze–thawing in phosphate buffer systems. J. Pharm. Sci. 91 (9), 1969–1979.
Pudipeddi, M., Zannou, E.A., Vasanthavada, M., Dontabhaktuni, A., Royce, A.E., Josh, Y. M., Serajuddin, A.T.M., 2008. Measurement of surface pH of pharmaceutical solids: a critical evaluation of indicator dye-sorption method and its comparison with slurry pH method. J. Pharm. Sci. 97 (5), 1831–1842.
Pyne, A., Chatterjee, K., Suryanarayanan, R., 2003. Solute Crystallization in Mannitol–Glycine Systems—Implications on Protein Stabilization in Freeze-Dried Formulations. J. Pharm. Sci. 92 (11), 2272–2283.
Pyne, A., Suryanarayanan, R., 2001. Phase transitions of glycine in frozen aqueous solutions and during freeze-drying. Pharm. Res. 18, 1448–1454.
Rodrigues, M.A., Rego, P., Geraldes, V., Connor, L.E., Oswald, I.D.H., Sztucki, M., Shalaev, E., 2021. Mannitol crystallization at sub-zero temperatures: time/temperature-resolved synchrotron X-ray diffraction study and the phase diagram. J. Phys. Chem. Lett. 12 (5), 1453–1460.
Roessl, U., Leitgeb, S., Nidetzky, B., 2015. Protein freeze concentration and micro-segregation analysed in a temperature-controlled freeze container. Biotechnol. Rep, 6, 108–111.
Samuelsen, L., Holm, R., Lathuile, A., Schönbeck, C., 2019. Buffer solutions in drug formulation and processing: how pKa values depend on temperature, pressure and ionic strength. Int. J. Pharm. 560, 357–364.
Slade, L., Harry, L., S., D., Reid, 1991. Beyond water activity: recent advances based on an alternative approach to the assessment of food quality and safety. Crit. Rev. Food Sci. Nutrit. 30(2-3): 115-360.
Su, W., Jia, N., Li, H., Hao, H., Li, C., 2017. Polymorphism of D-mannitol: crystal structure and the crystal growth mechanism. Chin. J. Chem. Eng. 25 (3), 358–362.
Sundaramurthi, P., Shalaev, E., Suryanarayanan, R., 2010. "pH swing" in frozen solutions-consequence of sequential crystallization of buffer components. J. Phys. Chem. Lett. 1 (1), 265–268.
Sundaramurthi, P., Suryanarayanan, R., 2011. Thermophysical properties of carboxylic and amino acid buffers at subzero temperatures: relevance to frozen state stabilization. J. Phys. Chem. B 115 (21), 7154–7164.
Sundberg, R.J., Martin, R.B., 1974. Interactions of histidine and other imidazole derivatives with transition metal ions in chemical and biological systems. Chem. Rev. 74 (4), 471–517.
Surovtsev, N.V., Adichtchev, S.V., Malinovsky, V.K., Ogienko, A.G., Drebushchak, V.A., Manakov, A.Y., Ancharov, A.I., Yunoshev, A.S., Boldyreva, E.V., 2012. Glycine phases formed from frozen aqueous solutions: revisited. J. Chem. Phys. 137 (6), 065103.
Susrisweta, B., Veselý, L., Štůsek, R., Hauptmann, A., Loerting, T., Heger, D., 2023. Investigating freezing-induced acidity changes in citrate buffers. Int. J. Pharm. 643, 123211.
Štůsek, R., Veselý, L., Melicharová, M., Zezula, J., Giebelmann, J., Loerting, T., Heger, D., 2024. Acidity and phase behavior of frozen hydrochloric acid during thawing. J. Phys. Chem. C.
Takenaka, N., Tanaka, M., Okitsu, K., Bandow, H., 2006. Rise in the pH of an unfrozen solution in ice due to the presence of NaCl and promotion of decomposition of gallic acids owing to a change in the pH. J. Phys. Chem. A 110 (36), 10628–10632.
Thorat, A.A., Munjal, B., Geders, T.W., Suryanarayanan, R., 2020. Freezing-induced protein aggregation - role of pH shift and potential mitigation strategies. J. Control. Release 323, 591–599.
Thorat, A.A., Suryanarayanan, R., 2019. Characterization of phosphate buffered saline (PBS) in frozen state and after freeze-drying. Pharm. Res. 36 (7), 98.
Towler, C.S., Davey, R.J., Lancaster, R.W., Price, C.J., 2004. Impact of molecular speciation on crystal nucleation in polymorphic systems: the conundrum of γ glycine and molecular 'self poisoning'. J. Am. Chem. Soc. 126 (41), 13347–13353.
Van den Berg, L., 1959. The effect of addition of sodium and potassium chloride to the reciprocal system-KH_2PO_4-Na_2HPO_4-H_2O on pH and composition during freezing. Arch. Biochem. Biophys. 84 (2), 305–315.
Van den Berg, L., 1966. pH changes in buffers and foods during freezing and subsequent storage. Cryobiology 3 (3), 236.

Van den Berg, L., Rose, D., 1959. Effect of freezing on the ph and composition of sodium and potassium phosphate solutions - the reciprocal system KH_2PO_4 - Na_2HPO_4 - H_2O. Arch. Biochem. Biophys. 81 (2), 319–329.
Varshney, D.B., Kumar, S., Shalaev, E.Y., Sundaramurthi, P., Kang, S.-W., Gatlin, L.A., Suryanarayanan, R., 2007. Glycine crystallization in frozen and freeze-dried systems: effect of pH and buffer concentration. Pharm. Res. 24 (3), 593–604.
Veselý, L., Susrisweta, B., Heger, D., 2021. Making good's buffers good for freezing: the acidity changes and their elimination via mixing with sodium phosphate. Int. J. Pharm. 593, 120128.
Veselý, L., Susrisweta, B., Štůsek, R., Mužík, D., Heger, D., 2025. Acidification of phosphate buffered saline. Int. J. Pharm. 676, 125593.
Veselý, L., Štůsek, R., Mikula, O., Yang, X., Heger, D., 2024a. Freezing-induced acidification of sea ice brine. Sci. Total Environ. 946, 174194.
Veselý, L., Závacká, K., Štůsek, R., Olbert, M., Neděla, V., Shalaev, E., Heger, D., 2024b. Impact of secondary ice in a frozen NaCl freeze-concentrated solution on the extent of methylene blue aggregation. Int. J. Pharm. 650, 123691.
Vetráková, Ľ., Neděla, V., Runštuk, J., Heger, D., 2019. The morphology of ice and liquid brine in an environmental scanning electron microscope: a study of the freezing methods. Cryosphere 13 (9), 2385–2405.
Vetráková, Ľ., Vykoukal, V., Heger, D., 2017. Comparing the acidities of aqueous, frozen, and freeze-dried phosphate buffers: is there a "pH memory" effect? Int. J. Pharm. 530 (1–2), 316–325.
Wade, A.M., Tucker, H.N., 1998. Antioxidant characteristics of L-histidine. J. Nutr. Biochem. 9 (6), 308–315.
Wang, W., 2000. Lyophilization and development of solid protein pharmaceuticals. Int. J. Pharm. 203 (1–2), 1–60.
Xavier, N.F.J., da Silva, A.M.J., Bauerfeldt, G.F., 2020. What rules the relative stability of α-, β-, and γ-glycine polymorphs? Cryst. Growth Des. 20 (7), 4695–4706.
Xu, W., Zhu, Q., Hu, C., 2017. The structure of glycine dihydrate: implications for the crystallization of glycine from solution and its structure in outer space. Angew. Chem. 129 (8), 2062–2066.